After cooling to room temperature, we added *p*-aminobenzoic acid ethyl ester, which reacts with ManNAc in the hydrolysate. The mixture was subsequently vortexed and then incubated in 80 °C for 1 h. After cooling the mixture to room temperature, equal volumes of distilled water and chloroform were added, and after vigorous vortexing, the mixture was centrifuged for 1 min. The *p*-aminobenzoic acid ethyl ester-converted monosaccharides in the upper aqueous layer were then analyzed by reversed-phase HPLC according to the manufacturer's instructions (Seikagaku Kogyo). To test the stability of *O*-acetylation of Ac_4ManNAc *in vivo*, we directly added *p*-aminobenzoic acid ethyl ester to the sample and analyzed the amount of *O*-acetyl-free ManNAc.

Animal Groups and Treatment Protocol—For subcutaneous Ac_4ManNAc treatment, we inserted a subcutaneous indwelling 2-French unit catheter at the back of anesthetized mice and connected this to a microinfusion pump system consisting of a Laboratory Animal Infusion kit (PUFC-C20-10, Instech Solomon, Plymouth Meeting, PA), a single axis counterbalanced swivel arm (CM375BP, Instech Laboratories), and an iPRECIO™ infusion pump (SMP101-L, Primetech, Tokyo, Japan). For this experiment, the DMRV/hIBM mice were grouped into three groups: low dose (SQAc4MN-LD) group with Ac_4ManNAc infused at a rate of 3 μl/h to deliver 40 mg/kg BW/day (n = 5), high dose group (SQAc4MN-HD) with Ac_4ManNAc infused at a rate of 10 μl/h to deliver 400 mg/kg BW/day (n = 4), and placebo (SQAc4MN-placebo) infused with plain normal saline (n = 5) at 3 μl/h. Unaffected control littermates (n = 14) whose genotypes are either $Gne^{+/-}$ or $Gne^{+/-}$h*GNE*D176V-Tg were likewise included in the cohort for analysis. We treated mice 15–23 weeks of age continuously for 23–25 weeks.

For oral Ac_4ManNAc treatment, DMRV/hIBM mice, including corresponding littermates, whose ages were 11–20 weeks were included in the cohort. The DMRV/hIBM mice were divided into three groups: placebo (n = 6) given acidic water, low dose (Ac4MN-LD) (n = 6) given Ac_4ManNAc at 40 mg/kg BW/day, and high dose (Ac4MN-HD) (n = 5) given Ac_4ManNAc at 400 mg/kg BW/day. Equal numbers of control littermates ($Gne^{+/-}$ or $Gne^{+/-}$h*GNE*D176V-Tg) per group were also treated (placebo, n = 6; Ac4MN-LD, n = 6; and Ac4MN-HD, n = 5). Ac_4ManNAc, computed according to the desired dose per day, was mixed with the drinking water and given continuously until the mice reached 54–60 weeks of age. In both subcutaneous and oral groups, blood was collected from the tail every month for plasma creatine kinase measurement and toxicology tests.

Analysis of Motor Performance—At the end of the treatment protocol, mice were exercised on a 10-lane treadmill (MK-680, Muromachi, Tokyo, Japan) with an adjustable belt speed and equipped with adjustable amperage shock bars at the rear of the belt. The mice were acclimatized to the treadmill with three 10-min running sessions at a 7° incline (5, 10, and 15 m/min) for 7 days after which two exercise tests were performed on separate days, a performance test and an endurance test. The performance test began with a speed of 15 m/min for 5 min and subsequently increased to 20 m/min, which was then gradually accelerated by 10 m/min every min until the mouse was exhausted and could no longer run. Exhaustion was defined as the inability of the mouse to return to the treadmill belt after 10 s on the shock bars despite electrostimulation. The time of exhaustion was used to calculate the distance that the mouse ran during the exercise. The endurance exercise consisted of a 60-min treadmill run at a constant speed of 20 m/min with a 7° incline after which the number of rests or beam breaks were recorded for 3 min. A digital video camera was positioned above the treadmill to record each test, and video recordings were used for analysis. Both tests were done three times with a 3–4-day rest in between.

Contractile Properties of Muscle—Measurement of muscle contractile properties of gastrocnemius and tibialis anterior muscles was performed according to previous protocols (22). All materials used for *in vitro* measurement of force were acquired from Nihon Kohden (Tokyo, Japan). After weighing the mice, they were deeply anesthetized with pentobarbital sodium (40 mg/kg) intraperitoneally and given supplemental doses as necessary to maintain adequate anesthesia, which was judged by the absence of response to tactile stimuli. The entire tibialis anterior and gastrocnemius muscles were isolated, removed, and secured with a 4-0 silk suture at the distal muscle tendon and proximal bone of origin after which the mice were sacrificed by cervical dislocation. Subsequently, the muscle was mounted in a vertical chamber that was connected to a force displacement transducer (TB-653T) and positioned between a pair of platinum electrodes that delivered an electrical stimulus. Throughout the analysis, the muscle was bathed in a physiological solution consisting of 137 mM NaCl, 24 mM $NaHCO_3$, 5 mM KCl, 2 mM $CaCl_2$, 1 mM $MgSO_4$, 11 mM glucose, 1 mM NaH_2PO_4, and 0.025 mM D-tubocurarine chloride; maintained at a temperature of 20 °C; and continuously perfused with a mixture of 95% O_2 and 5% CO_2 to maintain a pH of 7.4. Square wave pulses 0.2 ms in duration were generated by a stimulator (SEN-3301) and amplified (PP-106H). Muscle tension (length) was gradually adjusted to the length (L_0) that resulted in maximal P_t. With the muscle held at L_0 and the duration changed to 3 ms, the force developed during trains of stimulation pulses (10–200 Hz) was recorded, and the maximum absolute P_0 was determined. Absolute P_0 was normalized with the physiological cross-sectional area (CSA), which was computed as the product of the ratio of muscle weight, L_0, and density for mammalian skeletal muscle (1.066 mg/mm^3) to obtain specific forces (P_t/CSA and P_0/CSA). Data obtained were digitized and analyzed with a Leg-1000 polygraph system equipped with QP-111H software. After analysis of force generation, the muscles were removed from the chamber, trimmed off from bone and tendons, blotted dry, and weighed.

Skeletal Muscle Histochemistry and Morphological Analysis—Muscle tissues were processed for pathological analysis as reported previously (18, 20). Serial cryosections were stained with H&E, modified Gomori trichrome, and acid phosphatase according to standard procedures. Stained sections were visualized on a microscope (Olympus BX51, Olympus, Melville, NY), and digitized images (DP70, Olympus, Tokyo, Japan) were acquired for pathological analysis. We counted the number of rimmed vacuoles in six transverse 8-μm-thick cryosections (at

least 100 μm apart) stained with H&E on whole gastrocnemius sections for each group of mice.

For morphometric analyses, we stained sarcolemma of gastrocnemius muscle cryosections probed with caveolin-3 (rabbit polyclonal antibody, 610059, BD Transduction Laboratories) for 1 h followed by Alexa Fluor-conjugated goat IgG antibody to rabbit (Invitrogen) for 30 min and obtained six randomly selected digital images at ×200 magnification to evaluate single fiber CSA. From these images, individual fiber diameter was measured from 1,000–1,500 fibers with ImageJ software (National Institutes of Health), taking note of the shortest anteroposterior diameter of each myofiber.

Skeletal Muscle Immunohistochemical Analysis—We immunostained 6-μm-thick cryosections from gastrocnemius muscles using the primary Abs rat mAb to lysosome-associated membrane protein 2 (Lamp2) (clone ABL-93, Developmental Studies Hybridoma Bank), rabbit polyclonal Ab to Aβ1–42 (AB5078P, Millipore, Billerica, MA), and mAb to polyubiquitin (Enzo Life Sciences, Inc. Farmingdale, NY) following published protocols (18, 20). We applied appropriate secondary Ab labeled with Alexa Fluor dyes (Invitrogen) for 30 min at room temperature. Digitized images were captured with a laser-scanning microscope (Olympus) and used for analysis.

Preparation of Crude Membrane and Protein Fractions—After measurement of force, the organs were harvested, immediately frozen on dry ice, and kept at −80 °C until use. On the day of tissue processing, organs were crushed and homogenized using a Dounce homogenizer in a buffer containing 75 mM KCl, 10 mM Tris, 2 mM $MgCl_2$, 2 mM EGTA, and protease inhibitor mixture (Complete Mini protease inhibitor tablet, Roche Applied Science), pH 7.4. Equal amounts of homogenized tissues were centrifuged for 1 h at 30,000 × *g* at 4 °C. We used the pellet, which represented the membrane fractions, for sialic acid measurement and protein analysis. After two washes in the same buffer, one fraction of the pellet was resuspended in 50 mM H_2SO_4, sonicated, and subjected to sialic acid measurement. We used the other pelleted fraction for analysis of the total protein amount by extracting protein with SDS buffer (2% SDS, 10% glycerol, 10 mM EDTA, 5% 2-mercaptoethanol, 0.0625 M Tris-HCl, pH 6.8).

Two-dimensional PAGE—For the first dimension electrophoresis, membrane proteins were extracted with a solution that contained 0.5% Nonidet P-40 (Sigma), 5% 2-mercaptoethanol, ampholyte pH 3–10 (Bio-Lyte 3/10 ampholyte, Bio-Rad), and 8 M urea. Samples were applied to 4% polyacrylamide capillary gels containing 8 M urea, 0.5% Nonidet P-40, and ampholyte pH 3–10 (23). Samples were electrofocused at a constant voltage of 80 V for 30 min and then at 300 V for 120 min with 0.02 M H_2SO_4 (anode) and 0.04 M NaOH (cathode) solutions. After electrofocusing, gels were equilibrated with SDS buffer for 30 min and then placed horizontally on top of a 15% SDS-polyacrylamide gel. Second dimension electrophoresis was performed at a constant current of 25 mA. The gel was later blotted into PVDF membrane.

Immunoblotting—Samples other than for two-dimensional PAGE were homogenized in SDS buffer. After boiling, supernatants (8 μg) were electrophoresed on 5–15% gradient polyacrylamide gels (Perfect NT Gel, DRC), transferred onto PVDF membranes, blocked with 5% fat-free milk, and probed with the following Abs: anti-podocalyxin (goat polyclonal Ab, AF1556, R&D Systems), anti-actin (rabbit polyclonal Ab, 01867-96, Kantokagaku), anti-mouse neprilysin (NEP) (goat polyclonal, AF1126, R&D Systems), anti-α-sarcoglycan (αSG) (clone Ad1/20A6, NCL-a-SARC, Novocastra), anti-β-dystroglycan (βDG) (clone 43DAG1/8D5, NCL-b-DG, Novocastra), and anti-γ-sarcoglycan (γSG) (clone 35DAG/21B5, NCL-g-SARC, Novocastra). Appropriate HRP-conjugated secondary Abs were used according to the manufacturer's protocol. Results were visualized with ECL (ECL Western blotting detection reagents, GE Healthcare) and digitized by ImageQuant LAS 4000mini (GE Healthcare).

Transferrin Isoelectric Focusing—Transferrin isoelectric focusing was performed based on standard methods (24, 25) with some modifications. Ten microliters of plasma was saturated with a mixture of 0.1 M $NaHCO_3$ and 20 mM $FeCl_3$ for 1 h at room temperature. Iron-saturated plasma was then diluted 10 times with 5% ampholyte (pH 3–10), 30% glycerol, and distilled water. Samples (2 μl each) were then applied to a 6% SDS-polyacrylamide gel that contained 10% ampholyte (pH 3–10). Isoelectric focusing was done using 0.02 M NaOH as cathode buffer and 0.01 M H_3PO_4 as anode buffer with the following program: 80 V for 30 min, 300 V for 60 min, and then 500 V for 30 min. After isoelectric focusing, the gel was equilibrated with 0.7% acetic acid for 15 min and then transferred to PVDF. The membrane was probed with an Ab that recognized the N terminus of murine transferrin (Santa Cruz Biotechnology, Inc., Santa Cruz, CA) followed by appropriate secondary Ab.

Biochemical and Toxicology Assays—We measured plasma creatine kinase as described previously (18). We determined the activity of plasma alkaline phosphatase using the Japanese Society of Clinical Chemistry method (19) with *p*-nitrophenyl phosphate as substrate and ethylaminoethanol-HCl as buffer. We measured aspartate aminotransferase by determining the reduction of NADH (Kyowa Medics). We assayed blood urea nitrogen by an automatic clinical analyzer (Dri-Chem 3,500 V, Fuji Film). All measurements were done in triplicates.

Amyloid Quantification—For quantifying the amount of amyloid in myofibers, we fixed six 10-μm-thick cryosections (each section was 100 μm apart) from the gastrocnemius muscle in 4% paraformaldehyde for 10 min followed by postfixation in ice-cold methanol for 10 min at −20 °C. We immunostained sections with mouse mAb to amyloid β (Aβ) (clone 6E10, SIG-39320, Covance; 1:400 dilution). We counted only the positive signals within the myofibers in the whole gastrocnemius section.

We prepared samples for ELISA according to published protocols with slight modifications (19). Homogenized proteins were extracted using equal volumes of 0.4% diethylamine and 100 mM NaCl. We centrifuged samples at 100,000 × *g* for 1 h at 4 °C and neutralized the supernatant with 0.5 M Tris base, pH 6.8. We then used the supernatant for amyloid quantification with commercially available ELISA kits for Aβ1–42 (Wako) and Aβ1–40 (IBL) after brief vortexing. We normalized the amount of amyloid per mg of protein. For plasma amyloid, we

used 25 μl of thawed plasma. All analyses were performed in duplicates.

NEP Activity—NEP activity was measured in total homogenates from skeletal muscles according to previous reports (26–28) with slight modifications. Skeletal muscle cryosections were homogenized in 150 mM NaCl, 100 mM Tris-HCl, pH 7.8, 1% Triton X-100. Ten microliters of the supernatant (~40 μg) with or without 50 μM Phosphoramidon was mixed with 0.17 mM NEP substrate (*N*-benzyloxycarbonyl-alanyl-alanyl-leucyl-*p*-nitroanilide) in 10 mM HEPES and 25 milliunits/ml aminopeptidase M in a total volume of 200 μl. The mixture was incubated at 37 °C for 14 h, and the amount of chromogenic substrate released in the reaction, which reflects NEP activity, was measured by determining the absorbance at 405 nm and normalized with protein amount. Analyses were done in duplicates.

Statistical Analyses—All values are expressed as means ± S.E. (or ±S.D.) as appropriate. For survival analysis, we used the Kaplan-Meier method to draw the survival curve and used the log rank test to compare groups. For other analysis to determine significance among groups, we used one-way analysis of variance with Dunnett's post-test to compare the treatment group with the placebo group. We set the level of significance to $p < 0.05$ for all analyses.

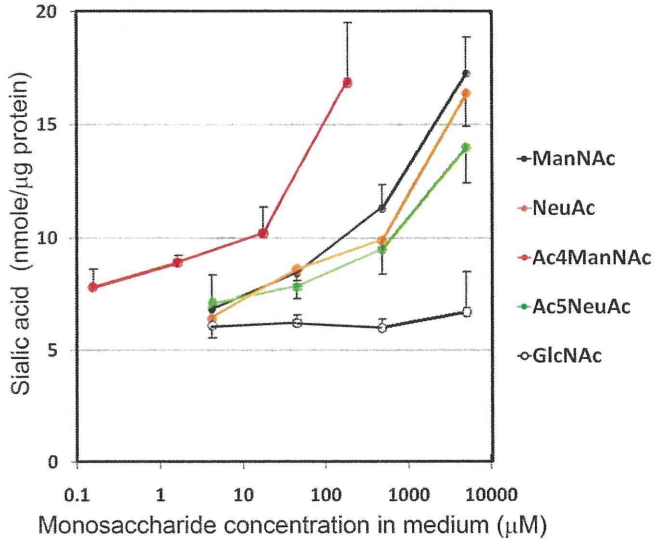

FIGURE 1. **Screening of compounds to increase cell sialylation.** Quantification of total sialic acid levels in DMRV/hIBM myotubes treated with increasing concentrations of monosaccharides is shown. Ac_4ManNAc shows a dose-dependent increment in total sialic acid levels; a sharp increase is seen between 20 and 200 μM, but a further increase in dose is limited by the toxicity of the compound. Total sialic acid levels are also increased by Ac_5NeuAc, ManNAc, and NeuAc, but the highest level required a dose 50 times higher than Ac_4ManNAc. *Error bars* represent S.E.

RESULTS

Screening of Peracetylated Monosaccharides to Increase Cellular Sialylation in DMRV/hIBM Myocytes—We examined the effect of three synthetic peracetylated ManNAc and NeuAc analogs, Ac_4ManNAc, Ac_5NeuAc, and Ac_5NeuAc-Me, on cellular sialylation in DMRV/hIBM patient myocytes. These agents were added into serum-free medium and compared with the natural compounds NeuAc and ManNAc. As treatment with Ac_4ManNAc (29) and Ac_5NeuAc-Me (data not shown) at concentration of 5 mM is known to cause decreased cell viability due to cell death by apoptosis, we checked the median lethal dose of both compounds on DMRV/hIBM cells and determined the LD_{50} to be 0.2 and 0.3 mM for Ac_4ManNAc and Ac_5NeuAc-Me, respectively (supplemental Fig. 1, A and B). Therefore, we used the concentrations of 0.2 and 0.3 mM for Ac_4ManNAc and Ac_5NeuAc-Me, respectively, and 5 mM for the other compounds.

Forty-eight hours after giving the various compounds, cells were subjected to immunohistochemical analysis. Myotubes obtained from the DMRV/hIBM and that were given GlcNAc as control were strongly stained with soy bean agglutinin lectin, which recognizes peripheral β-*N*-acetylgalactosaminide structure, and faintly stained with wheat germ agglutinin lectin, which recognizes a cluster of sialic acids (supplemental Fig. 1C); this pattern of staining reflects hyposialylation of cells. In contrast, cells maintained in serum-free conditions and given Ac_4ManNAc and Ac_5NeuAc exhibited increased cellular sialylation, similar to that with ManNAc and NeuAc, by showing the opposite pattern: faint staining with soybean agglutinin and strong staining with wheat germ agglutinin. However, it is important to note that these lectin binding patterns, although not definitive, are consistent with increased sialylation for certain test compounds. The staining pattern of improved sialylation was also seen in cells incubated in 10% FBS but not in the cells given Ac_5NeuAc-Me. Similar results were obtained in the myocytes from DMRV/hIBM mouse (supplemental Fig. 2).

By quantifying the change in sialylation levels after treatment with various compounds, Ac_4ManNAc was found to have the most robust effect in DMRV/hIBM myocytes (Fig. 1). Total sialic acid levels were also increased by Ac_5NeuAc, ManNAc, and NeuAc in a dose-dependent fashion, but the highest level was obtained using a dose 50 times higher than that of Ac_4ManNAc. Thus, in the succeeding *in vivo* studies, we evaluated Ac_4ManNAc and its effect on increasing sialylation in various tissues.

Ac_4ManNAc Displays Rapid Rate of Excretion into Urine—To determine the most effective route of administration, we gave a single dose (31 μmol) of Ac_4ManNAc by intravenous, intraperitoneal, subcutaneous, and intragastric routes to wild type mice and collected serum and urine samples at specified periods for analysis. The peak levels of ManNAc derivatives were found in the serum at 5 min via intravenous route, 10 min via intraperitoneal and subcutaneous routes, and 30 min via intragastric route (Fig. 2*A*). At 120 min, most of the ManNAc derivatives were detectable in the serum only in the intragastric group. The amount of ManNAc derivatives gradually declined over time and became virtually undetectable after 240 min. Of note, the derivatives reached a plateau in the subcutaneous route between 10 and 30 min before a gradual decrease as compared with the rapid decline in the other routes.

In terms of excretion, the peak of ManNAc derivatives was detected earliest in the urine by intravenous route at 5 min followed by the intraperitoneal and subcutaneous routes at 30 min and intragastric route at 60 min. After the peak levels, ManNAc derivatives gradually declined and were undetectable after 4 h except for the subcutaneous route where some derivatives were detectable up to 8 h (Fig. 2*B*). These results demon-

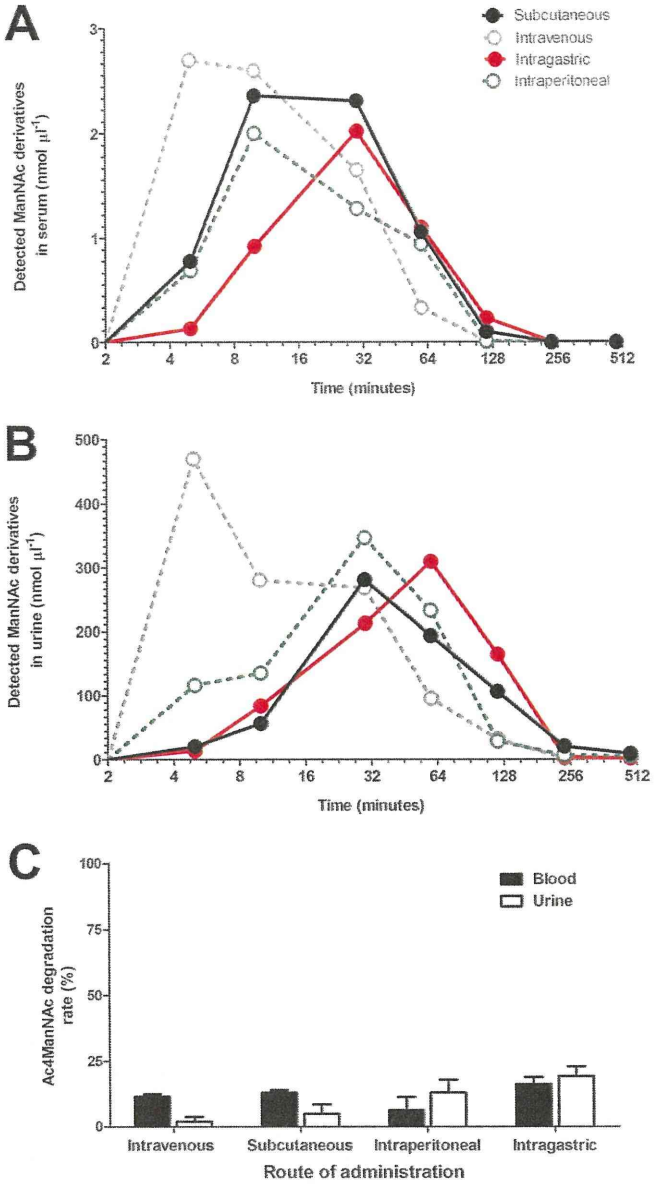

FIGURE 2. **Pharmacokinetics of Ac_4ManNAc.** *A*, after a single dose of 31 μmol of Ac_4ManNAc, the peak levels of ManNAc derivatives are seen in the serum at 5 min (intravenous), 10 min (intraperitoneal and subcutaneous), and 30 min (intragastric). After 120 min, most ManNAc derivatives are detectable only in the intragastric group. *B*, the levels of ManNAc derivatives in urine, reflecting Ac_4ManNAc, are shown. Earliest detection is seen in the intravenous route followed by the intraperitoneal and subcutaneous routes. The peak for the intragastric route appeared last. A gradual decline in ManNAc derivatives is seen after the peak levels, and these become undetectable after 4 h except for the subcutaneous route where some derivatives are still seen up to 8 h. *C*, *O*-acetylation status of Ac_4ManNAc calculated by measuring the ManNAc derivatives in serum or urine collected during the peak levels with or without hydrolysis reflecting the degradation rate of the compound administered. In all routes of administration used, the degradation rate was ~15–20% in both blood (*closed bars*) and urine (*white bars*), indicating that more than 80% of Ac_4ManNAc was estimated to maintain its *O*-acetylation status.

strate that administered Ac_4ManNAc after being absorbed into the blood is rapidly excreted into the urine similar to ManNAc and NeuAc (19) and imply that continuous or frequent administration of Ac_4ManNAc is needed to maintain effective levels in blood. Of the four routes, however, intragastric and subcutaneous routes appear to have a slower excretion rate.

To determine the extent to which Ac_4ManNAc is subjected to esterases in the circulation, we checked the *O*-acetylation status of administered Ac_4ManNAc by measuring the detection rate of ManNAc in serum or urine (at peak of detection) with or without hydrolysis. In all routes of administration used, more than 80% of Ac_4ManNAc was estimated to maintain its *O*-acetylation status in both blood and urine (Fig. 2*C*). Interestingly, when we incubated Ac_4ManNAc in the blood for 30–60 min at room temperature, the *O*-acetylation rate of Ac_4ManNAc was significantly decreased (data not shown).

Subcutaneous Infusion of Ac_4ManNAc Increases Sialic Acid in Plasma and Tissues in DMRV/hIBM Mice—To check whether Ac_4ManNAc can be used to increase sialic acid in DMRV/hIBM mice *in vivo*, we performed a pilot study to evaluate whether Ac_4ManNAc can be incorporated in murine tissues without causing undue toxicity. As our results on the pharmacokinetics suggested that the preferred routes of administration are either subcutaneous or intragastric, we continuously infused Ac_4ManNAc subcutaneously using an infusion pump with the tip of the catheter surgically placed under dorsal skin in three groups of DMRV/hIBM mice that received either Ac_4ManNAc at 40 mg/kg BW/day (SQAc4MN-LD), Ac_4ManNAc at 400 mg/kg BW/day (SQAc4MN-HD), or plain normal saline (SQAc4MN-placebo). After 25 weeks, we analyzed sialic acid levels in tissues of treated mice. The bound forms of sialic acid were remarkably increased in almost all organs, including skeletal muscle, liver, heart, kidney, lung, spleen, brain, and plasma with dose dependence in DMRV/hIBM mice, except the intestine (Fig. 3). Notably, the increase in sialylation was more evident as compared with our previous study using natural compounds (19). Incidentally, subcutaneous treatment with Ac_4ManNAc improved the survival rate (supplemental Fig. 3A) and prevented weight loss (supplemental Fig. 3B) in SQAc4MN-LD and SQAc4MN-HD as compared with SQAc4MN-placebo.

Oral Ac_4ManNAc Improves Survival and Prevents Onset of Muscle Atrophy, Weakness, and Degeneration in DMRV/hIBM Mice—As the increase in sialic acid levels was more remarkable and dose-dependent with Ac_4ManNAc as compared with natural compounds, we analyzed the effects of Ac_4ManNAc using the oral route in three groups of DMRV/hIBM mice: low dose (Ac4MN-LD; 40 mg/kg BW/day), high dose (Ac4MN-HD; 400 mg/kg BW/day), and non-treated (placebo; plain acidic water). For a control, the same number of littermates was used for each group (littermate Ac4MN-LD, littermate Ac4MN-HD, and littermate placebo). Treatment with oral Ac_4ManNAc improved the survival and BW in the DMRV/hIBM Ac4MN-LD group as compared with DMRV/hIBM placebo, but a more remarkable treatment effect was seen in the DMRV/hIBM Ac4MN-HD group (Fig. 4, *A* and *B*). Treated DMRV/hIBM mice showed an increase in weight (Fig. 4*C*) and physiologic CSA (Fig. 4*D*) of gastrocnemius muscles and tibialis anterior muscles (data not shown). Of note, BW and gastrocnemius mass of DMRV/hIBM mice were recovered to levels similar to littermates after treatment. DMRV/hIBM mice in both Ac_4MN-LD and Ac4MN-HD groups performed better than DMRV/hIBM placebo in running on a treadmill and enduring a specific running workload (Fig. 4, *E* and *F*). Furthermore, *ex vivo* measurement of force in

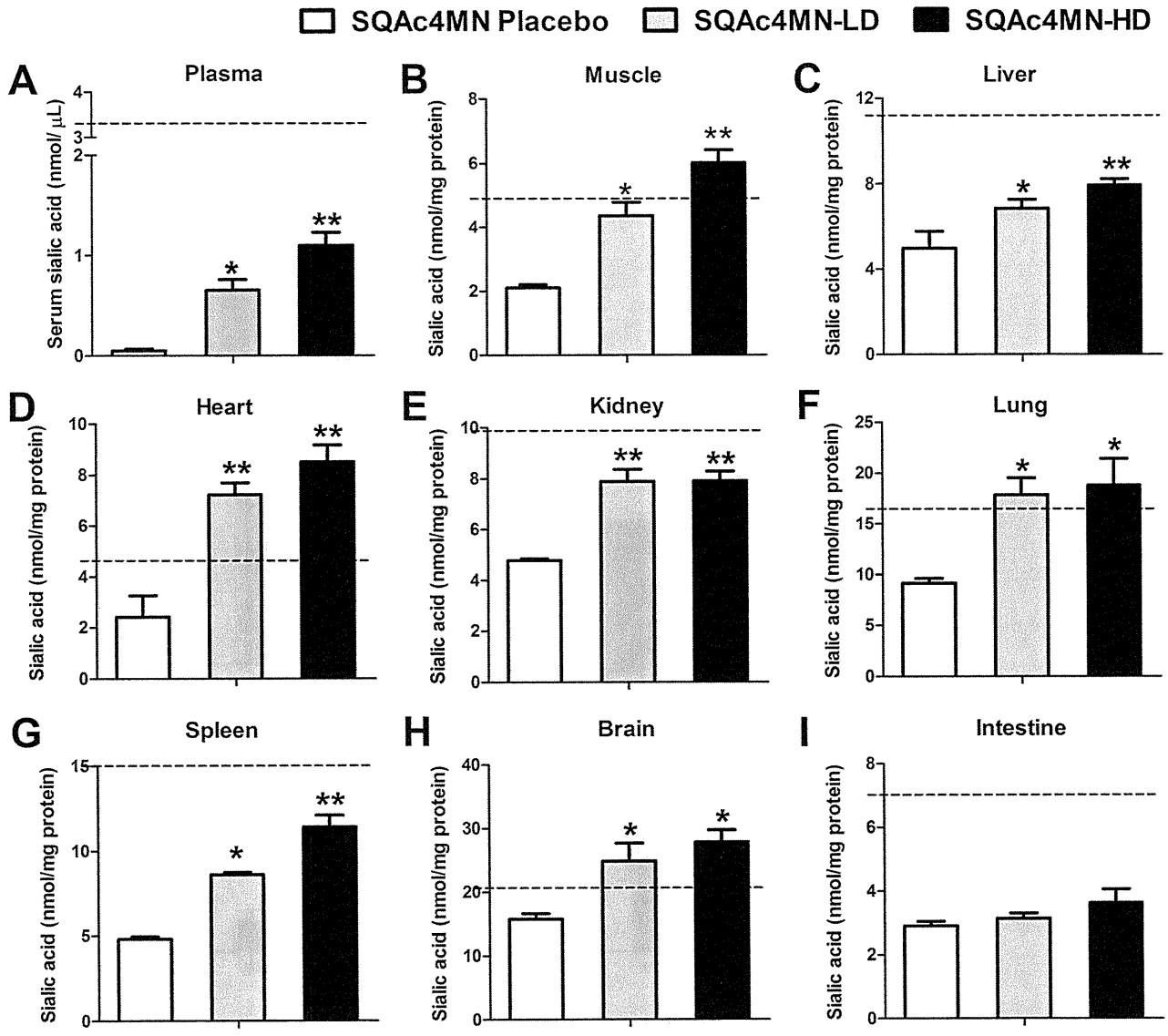

FIGURE 3. **Subcutaneous delivery of Ac_4ManNAc increases sialic acid in plasma and tissues.** Total sialic acid levels in plasma (*A*) and membrane-bound sialic acid levels in skeletal muscle (*B*), liver (*C*), heart (*D*), kidney (*E*), lung (*F*), spleen (*G*), brain (*H*), and intestine (*I*) after 25 weeks of subcutaneous infusion are shown in three groups DMRV/hIBM mice: DMRV/hIBM placebo (PBS; *open bars*), SQAc4MN-LD (40 mg/kg BW/day; *gray bars*), and SQAc4MN-HD (400 mg/kg BW/day; *black bars*). Sialic acid levels are remarkably increased in a dose-dependent manner in plasma and most tissues except the intestines. *Dotted horizontal lines* represent mean sialic acid levels in untreated littermates. *Single asterisks* (*) indicate $p < 0.05$ (DMRV/hIBM placebo *versus* treated DMRV/hIBM); *double asterisks* (**) indicate $p < 0.001$. *Error bars* represent S.E.

isolated muscles showed a marked increase not only in the peak isometric (P_t) and peak tetanic forces (P_0) (data not shown) but more importantly also in both the specific isometric force (P_t/CSA) (Fig. 4*G*) and specific tetanic force (P_0/CSA) (Fig. 4*H*) after treatment. P_t/CSA and P_0/CSA increments in DMRV/hIBM mice in Ac4MN-LD and Ac4MN-HD groups paralleled the increase in single fiber diameter as evidenced by a rightward shift of individual muscle fiber diameters, which also indicate a smaller number of atrophic fibers (Fig. 4*I*).

When comparing DMRV/hIBM Ac4MN-LD and Ac4MN-HD groups, dose-response correlation was noted in treadmill motor performance, endurance test, and P_t/CSA in gastrocnemius muscle. Additionally, Ac_4ManNAc treatment decreased plasma creatine kinase levels from 823.3 ± 30.0 IU/liter in non-treated DMRV mice to 270.0 ± 38.0 and 240.0 ± 84.3 IU/liter in treated mice with the low dose and high dose, respectively (supplemental Fig. 3). In all parameters tested, the littermates that were included in Ac_4MN-LD and Ac4MN-HD groups maintained levels similar to those of non-treated littermate placebo, further indicating that treatment was not detrimental to mice at least in the doses used in this study.

In terms of toxicity, the blood urea nitrogen, plasma aspartate aminotransferase, and plasma alkaline phosphatase levels, which reflect kidney and liver functions, were within normal ranges in all mice treated (Table 1). As the use of Ac_4ManNac in cells has been associated with cell toxicity (supplemental Fig. 1), we analyzed several tissues after treatment with Ac_4ManNAc with regard to reactivity to TUNEL staining but did not find any difference between treatment and placebo groups, indicating the absence of overt signs of toxicity (data not shown) and

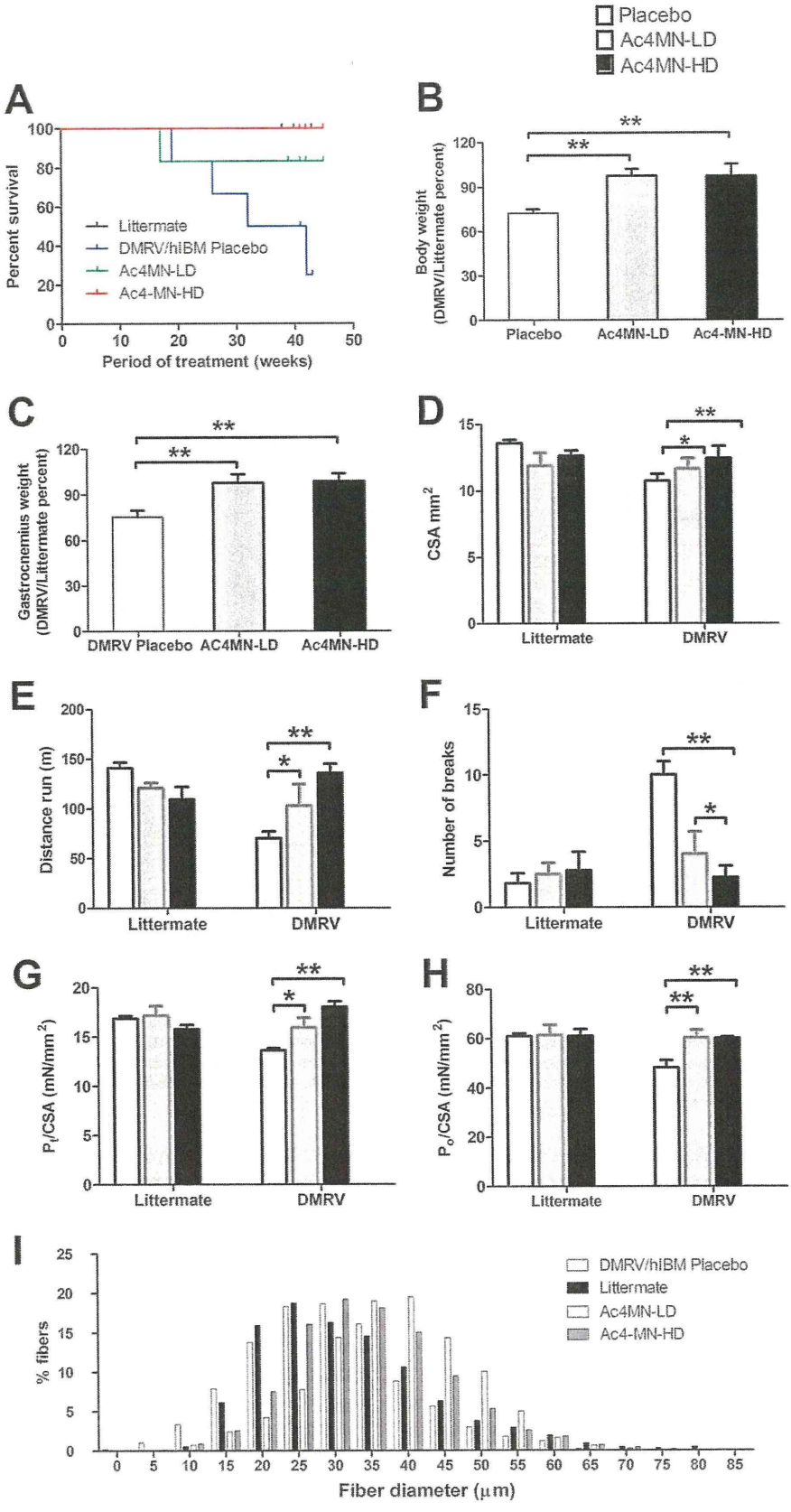

TABLE 1
Kidney and liver function tests after Ac_4ManNAc
AST, plasma aspartate aminotransferase; ALP, plasma alkaline phosphatase; BUN, blood urea nitrogen.

Group	AST (mean ± S.E.)	ALP (mean ± S.E.)	BUN (mean ± S.E.)
	IU/liter	*IU/liter*	*mg/dl*
Littermate	13.20 ± 4.09	47.22 ± 4.11	92.47 ± 12.22
DMRV/hIBM placebo	12.83 ± 3.81	39.14 ± 4.72	107.60 ± 9.61
DMRV/hIBM Ac4MN-LD	14.82 ± 2.88	49.25 ± 2.88	92.44 ± 8.04
DMRV/hIBM Ac4MN-HD	12.91 ± 4.01	51.84 ± 3.65	91.01 ± 13.04

implying that Ac_4ManNAc might be tolerated by mice over a prolonged period of administration.

Administration of Ac_4ManNAc Prevents Intracellular Inclusions and Rimmed Vacuole Formation in Myofibers—Gastrocnemius muscles of non-treated DMRV/hIBM (DMRV/hIBM placebo) mice show several rimmed vacuoles (*arrow*) and intracellular deposits (*arrowhead*) in myofibers (Fig. 5*A*, *upper panel*). Enhanced acid phosphatase activity was also observed around rimmed vacuoles, suggesting the presence of acidic organelles that may represent autophagic vacuoles (18). These changes in muscle pathology were not observed in treated or non-treated control littermates (data not shown). Oral treatment in Ac4MN-LD and Ac4MN-HD groups led to a marked reduction in the number of rimmed vacuoles and reactivity to acid phosphatase staining in muscle cryosections (Fig. 5*A*, *middle* and *lower panels*). Quantitative analysis showed that the number of rimmed vacuoles in DMRV/hIBM Ac4MN-LD (Fig. 5*B*) was significantly lower than in DMRV/hIBM placebo, whereas none were seen in DMRV/hIBM Ac4MN-HD. In addition, the number of rimmed vacuoles in Ac4MN-LD DMRV/hIBM was actually lower when compared with NeuAc and ManNAc treatment (19).

Immunoreactive signals to Lamp2, a marker for lysosome; Aβ1–42, which recognizes one of the Aβ peptides; and polyubiquitin were observed in muscles of DMRV/hIBM placebo (Fig. 6*A*) but were not seen in control littermates (data not shown). The signals of those proteins were hardly observed in DMRV/hIBM mice after oral treatment (Fig. 6*A*, Ac4MN-LD and Ac4MN-HD). The immunoreaction to other proteins such as amyloid precursor protein, Aβ1–40, neurofilament proteins, phosphorylated tau, microtubule-associated protein light chain 3 (LC3; a marker for autophagosome), endoplasmin (GRP94, a marker of endoplasmic reticulum stress), and dystrophin-associated proteins, which are accumulated in myofibers of DMRV/hIBM mice (18), also disappeared after oral Ac_4ManNAc treatment (data not shown). Quantification of the number of fibers with rimmed vacuoles and Aβ inclusions also showed a significant decrease in Ac4MN-LD, but these were undetectable in Ac4MN-HD (supplemental Fig. 4). The amount of LC3-II was also reduced by Ac_4ManNAc treatment (data not shown).

Sialic Acid in Plasma and Various Organs Is Increased by Oral Ac_4ManNAc Treatment—After oral treatment, sialic acid was markedly increased in the plasma and other organs of DMRV/hIBM mice in a dose-dependent manner (Fig. 7). In the littermates included in the Ac4MN-LD and Ac4MN-HD groups, the levels of membrane-bound sialic acid were also increased when compared with the littermate placebo levels. Notably, however, levels in treated DMRV/hIBM mice were much higher than those of non-treated littermate placebo with the most prominent effects seen in lung, spleen, and brain (Fig. 7, *F–H*). In addition, higher levels of sialylation were achieved in the mice treated through the oral route as compared with the subcutaneous route (compare Fig. 7 with Fig. 3). Again, the sialic acid levels of all organs recovered after oral Ac_4ManNAc treatment were higher than those after ManNAc and NeuAc treatment (19).

Sialylation of Glycoproteins in DMRV/hIBM Mice Is Improved by Ac_4ManNAc Treatment—Hyposialylation of some muscle glycoproteins has been reported in DMRV/hIBM muscles (26, 30, 31). In this study, we evaluated the sialylation status of αSG, βDG, and NEP by two-dimensional PAGE analysis of skeletal muscle membrane proteins of non-treated littermates and DMRV/hIBM mice who were given either placebo, Ac4MN-LD, or Ac4MN-HD (Fig. 8*A*). In DMRV/hIBM placebo, when compared with non-treated littermates, the spots for αSG were shifted to the right (Fig. 8*B*) in reference to γSG (a non-sialylated protein), indicating αSG hyposialylation. The pattern of βDG staining was not changed. After treatment, in both Ac4MN-LD and Ac4MN-HD, αSG spots were notably shifted back to the left, indicating recovery of sialylation. In non-treated littermates, the NEP pattern comprised two spots, but in DMRV/hIBM placebo, spot 1 was not detected, whereas spot 2 was shifted to the right (basic). After treatment, however, NEP spot 1 became visible and was shifted back to the left side (acidic) together with spot 2 (Fig. 8*B*).

In addition to these membrane proteins, podocalyxin, the major podocyte sialoprotein, was shown to be hyposialylated in homozygous mutant *Gne* knock-in mice ($Gne^{M712T/M712T}$) (32). In the kidney and skeletal muscle of DMRV/hIBM mice, podocalyxin from DMRV/hIBM placebo mice was indeed hyposialylated, migrating more slowly than littermate control (supplemental Fig. 5, A and B). Ac_4ManNAc treatment led to more rapid dose-dependent migration as compared with DMRV/hIBM placebo, suggesting the recovery of sialylation.

In the serum, several glycoproteins are known to be sialylated, including transferrin, α_1-antitrypsin, α_1-acid glycopro-

FIGURE 4. **Oral treatment of Ac_4ManNAc improves survival and prevents onset of muscle weakness and atrophy in DMRV/hIBM mice.** Three groups of mice were Ac4MN-LD (40 mg/kg BW/day) (*gray bars*), Ac4MN-HD (400 mg/kg BW/day) (*black bars*), and placebo (plain acidic water) (*white bars*). Improvement in survival (*A*) and BW (*B*) is seen in Ac4MN-HD more than Ac4MN-LD as compared with DMRV/hIBM placebo. Isolated gastrocnemius muscles had increases in weight (*C*) and CSA (*D*) in treated DMRV/hIBM mice. In terms of motor performance, DMRV/hIBM mice in Ac4MN-LD and Ac4MN-HD groups performed better than the DMRV/hIBM placebo group in running on a treadmill (*E*) and endurance (*F*). *Ex vivo* measurement of force revealed a marked increase in P_t/CSA (*G*) and P_o/CSA (*H*) in treated DMRV/hIBM mice. A rightward shift of individual muscle fiber diameters in DMRV/hIBM mice (*I*) is seen after treatment; this also indicates a smaller number of atrophic fibers. *Single asterisks* (*) indicate $p < 0.05$; *double asterisks* (**) indicate $p < 0.001$. *Error bars* represent S.E.

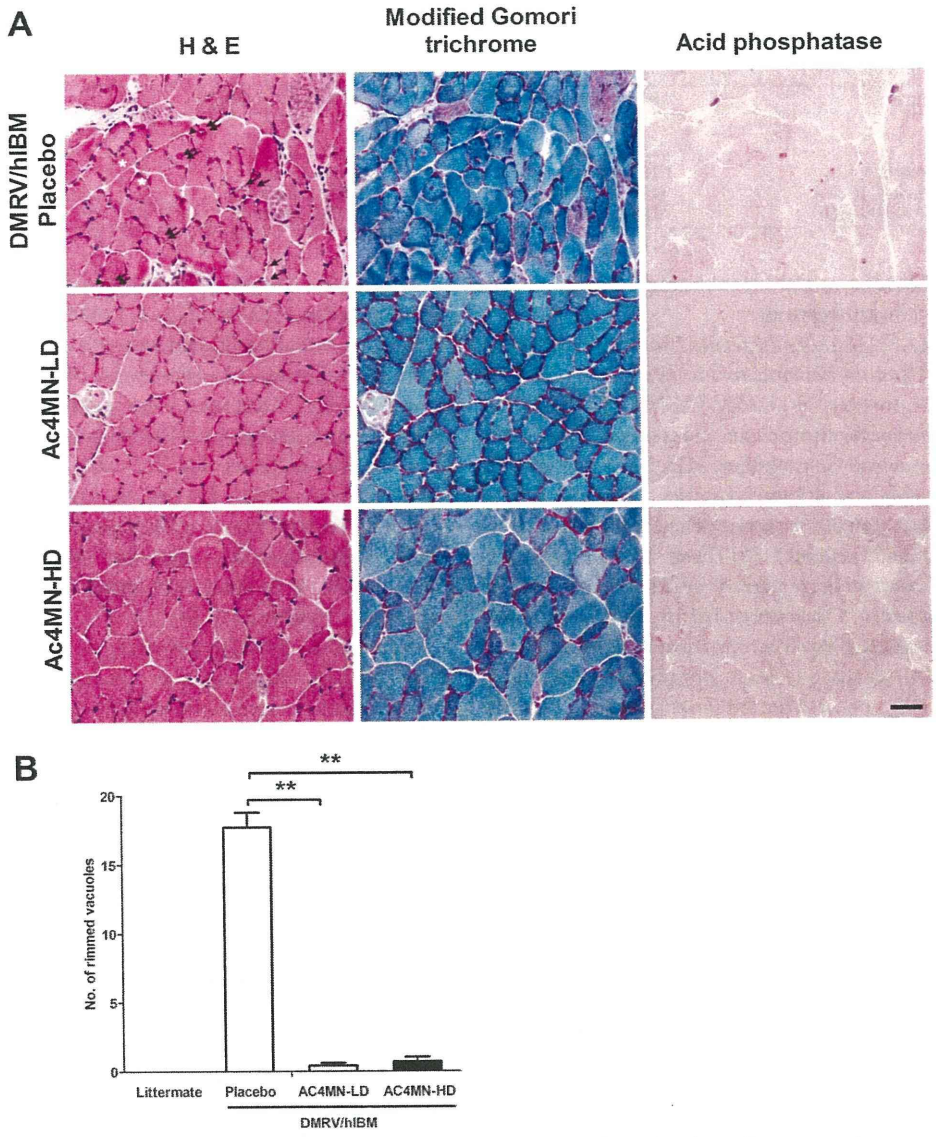

FIGURE 5. **Oral treatment with Ac_4ManNAc prevents appearance of rimmed vacuoles.** *A*, histochemistry of gastrocnemius cryosections from DMRV/hIBM mice in treated and placebo groups is shown. In the placebo group, H&E staining shows variations in fiber size, scattered atrophic fibers (*arrows*), fibers with rimmed vacuoles (*double arrows*) and inclusions (*arrowhead*), and some fibers with internal nucleation (*asterisk*). Modified Gomori trichrome staining highlights rimmed vacuoles within the fibers. Acid phosphatase staining is also highlighted in fibers with rimmed vacuoles and small atrophic fibers due to the presence of acidic organelles that may represent autophagic vacuoles. These pathologies are not seen in the gastrocnemius muscles of both Ac4MN-LD and Ac4MN-HD. *Bar*, 50 μm. *B*, quantitative analysis of rimmed vacuoles in gastrocnemius cryosections of non-treated control littermates (*dark gray bars*), non-treated DMRV/hIBM (*white bars*), DMRV/hIBM treated with low dose Ac_4ManNAc (Ac4MN-LD; *light gray bars*), and DMRV/hIBM treated with high dose Ac_4ManNAc (Ac4MN-LD; *black bars*). *Double asterisks* indicate $p < 0.001$. *Error bars* represent S.E.

tein, immunoglobulin G, and fibrinogen, none of which have been fully evaluated for altered sialylation level in DMRV/hIBM. In this study, we checked the sialylation pattern of transferrin in iron-saturated plasma. In littermates, the predominant tetrasialotransferrin was readily observed in addition to faint pentasialotransferrin; in contrast, DMRV/hIBM placebo mice express the asialotransferrin (non-sialylated) isoform in addition to di- and trisialotransferrin isoforms (Fig. 9*A*). We also confirmed the recovery of sialylation of transferrin in plasma of Ac_4ManNAc-treated DMRV/hIBM mouse seen as an increase in the quantity of tri- and tetrasialotransferrin and disappearance of asialotransferrin in Ac_4ManNAc-treated DMRV/hIBM (Ac4MN-LD and Ac4MN-HD) mice as compared with DMRV/hIBM placebo (Fig. 9, *A* and *B*).

Increase in Amyloid Burden in DMRV/hIBM Mice May Be Related to Decreased NEP Activity and Is Reversed by Treatment with Ac_4ManNAc—Quantitative measurement of amyloid by amyloid ELISA showed that Aβ1–40 and Aβ1–42 levels are increased in DMRV/hIBM placebo as compared with littermates in both plasma (Fig. 10*A*) and muscle (Fig. 10*B*). After treatment, the Aβ1–40 and Aβ1–42 levels were reduced in both Ac4MN-LD and Ac4MN-HD. To understand the mechanism by which Aβ peptides are generated in DMRV/hIBM, we measured β-secretase (generating enzyme) and NEP (catabolizing enzyme) activities, which are hypothesized to up-regulate Aβ levels (26, 33). β-Secretase activity was not changed in DMRV/hIBM mouse muscle (data not shown), whereas the activity of NEP was decreased (Fig. 10*C*). By Ac_4ManNAc treat-

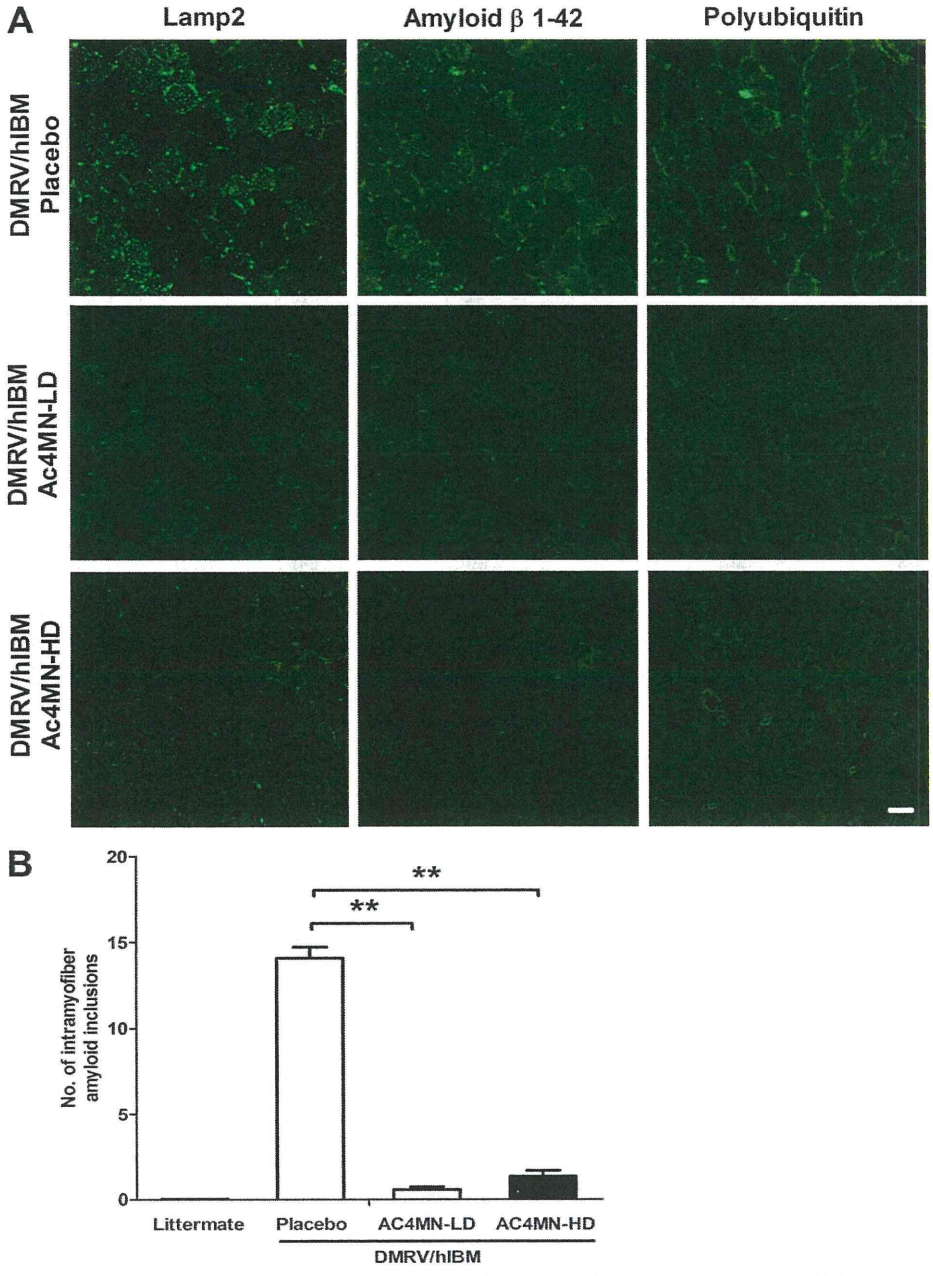

FIGURE 6. **Oral treatment with Ac_4ManNAc prevents occurrence of intracellular inclusions in DMRV/hIBM myofibers.** *A*, in muscle cryosections from non-treated DMRV/hIBM mice (DMRV placebo), immunoreactive signals to Lamp2, Aβ1–42, and polyubiquitin were seen within myofibers. In Ac4MN-LD and Ac4MN-HD groups, immunoreactivities to Lamp2, Aβ1–42, and polyubiquitin were not seen. *Bar*, 50 μm. *B*, quantitative analysis of amyloid deposits myofibers counted in several cryosections and averaged in non-treated control littermates (*dark gray bars*), non-treated DMRV/hIBM (*white bars*), DMRV/hIBM treated with low dose Ac_4ManNAc (Ac4MN-LD; *light gray bars*), and DMRV/hIBM treated with high dose Ac_4ManNAc (Ac4MN-LD; *black bars*) shows an increase of amyloid deposits in non-treated DMRV placebo that is markedly reduced in Ac4MN-LD and Ac4MN-HD groups after treatment. *Double asterisks* indicate $p < 0.001$. *Error bars* represent S.E.

ment, NEP activities in both Ac4MN-LD and Ac4MN-HD DMRV/hIBM mice were recovered to values similar to that in littermates (Fig. 10*C*). These results imply that neprilysin may be the major enzyme related to Aβ metabolism that can be affected by cellular hyposialylation. The NEP amount as detected by Western blot analysis was not influenced by mouse genotype or treatment (data not shown).

DISCUSSION

We have recently reported the prophylactic effect of ManNAc on myopathy of DMRV/hIBM mice but did not observe a dose-effect correlation in using three doses of ManNAc (19). In the present study, we provide evidence that Ac_4ManNAc can remarkably increase cellular sialylation *in vivo* and in a dose-dependent manner, resulting in a more robust effect on preventing the myopathic phenotype in the DMRV/hIBM mouse as compared with natural sialic acid metabolites.

It has been reported that extrinsic acylated monosaccharides can be effectively incorporated into the sialic acid biosynthetic pathway by modifying metabolic flux in the cells (34–37) to modulate the structure and function of sialic acid-bearing gly-

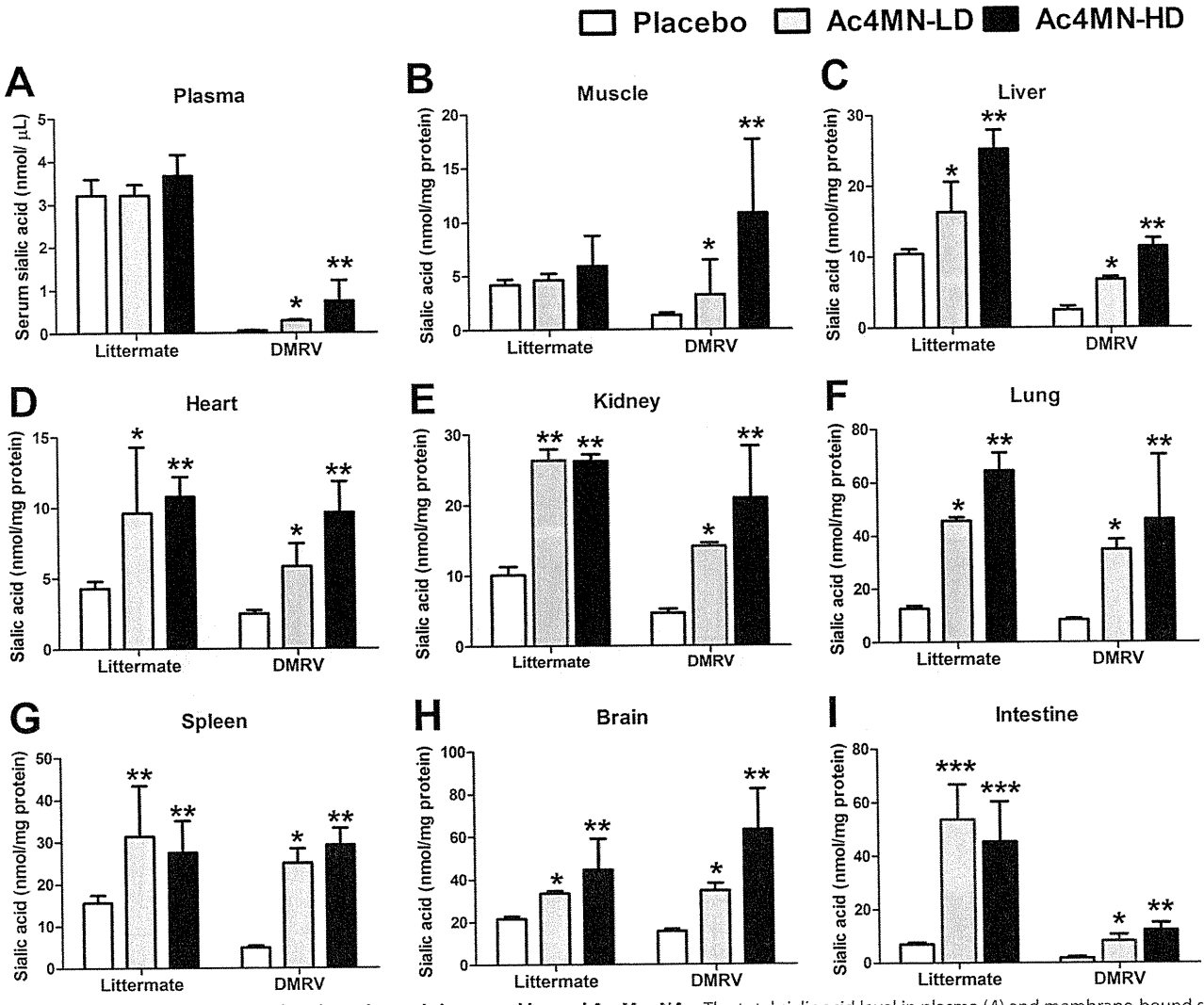

FIGURE 7. **Sialylation of plasma and various tissues is increased by oral Ac_4ManNAc.** The total sialic acid level in plasma (*A*) and membrane-bound sialic acid levels in skeletal muscle (*B*), liver (*C*), heart (*D*), kidney (*E*), lung (*F*), spleen (*G*), brain (*H*), and intestine (*I*) after treatment with oral Ac_4ManNAc given daily for 42–43 weeks are shown. Both DMRV and littermates were divided into three groups: placebo (acidic water), Ac4MN-LD (40 mg/kg/day; *gray bars*), and Ac4MN-HD (400 mg/kg/day; *black bars*). Note the dose-dependent increase in sialic acid levels when comparing Ac4MN-LD and Ac4MN-HD in DMRV mice. *Single asterisks* (*) indicate $p < 0.05$ (DMRV placebo *versus* treated DMRV and littermate *versus* treated littermate); *double asterisks* (**) indicate $p < 0.001$ (DMRV placebo *versus* treated DMRV and littermate *versus* treated littermate). *Error bars* represent S.E.

coproteins and lipids (38). We screened three commercially available synthetic peracetylated monosaccharides for an increase in cellular sialylation of cultured DMRV/hIBM myocytes and observed that DMRV/hIBM cells have the ability to incorporate these exogenous molecules, like ManNAc and NeuAc, and flux them into the cellular sialic metabolic pathway, coinciding with the findings in previous reports (16, 29, 36). In screening for the most effective compound, we found that Ac_4ManNAc had the strongest effect on increasing sialylation even when using a comparably lower dose than the other compounds, although it induced cell death when given in higher doses, corresponding to findings reported in some cell lines (29, 35, 36).

ManNAc can be modified either at its *O*-acyl site or *N*-acyl site. The use of *O*-acyl-modified (peracetylated) ManNAc analogs has been shown to increase metabolic efficiency up to 900-fold (35), and among these, Ac_4ManNAc was the most efficient in increasing total sialic acid levels (34). This distinct efficiency exhibited by Ac_4ManNAc may be explained by two factors. First, *O*-acetylation of ManNAc provides hydrophobic modifications on the hydroxyl groups of the molecule because of the properties endowed by acetyl esters that facilitate passive diffusion of the compound into a cell (39). Second, *O*-acyl ManNAc analogs are believed to be sequestered in cellular membranes that serve as a "reservoir" for these compounds (35) as only a minor fraction is believed to be converted by cells to sialic acid. *N*-Acyl modifications (not used in this study) can also increase cell sialylation (40); increasing the side chains further, however, can lead to decreased sialic acid production and lower metabolic flux (35).

A caveat to the increased metabolic efficiency of hydroxyl-modified or peracetylated sugar analogs, however, is decreased cell viability upon increasing the dose or increasing the number of carbon atoms that is attributed in part to apoptosis (29). But

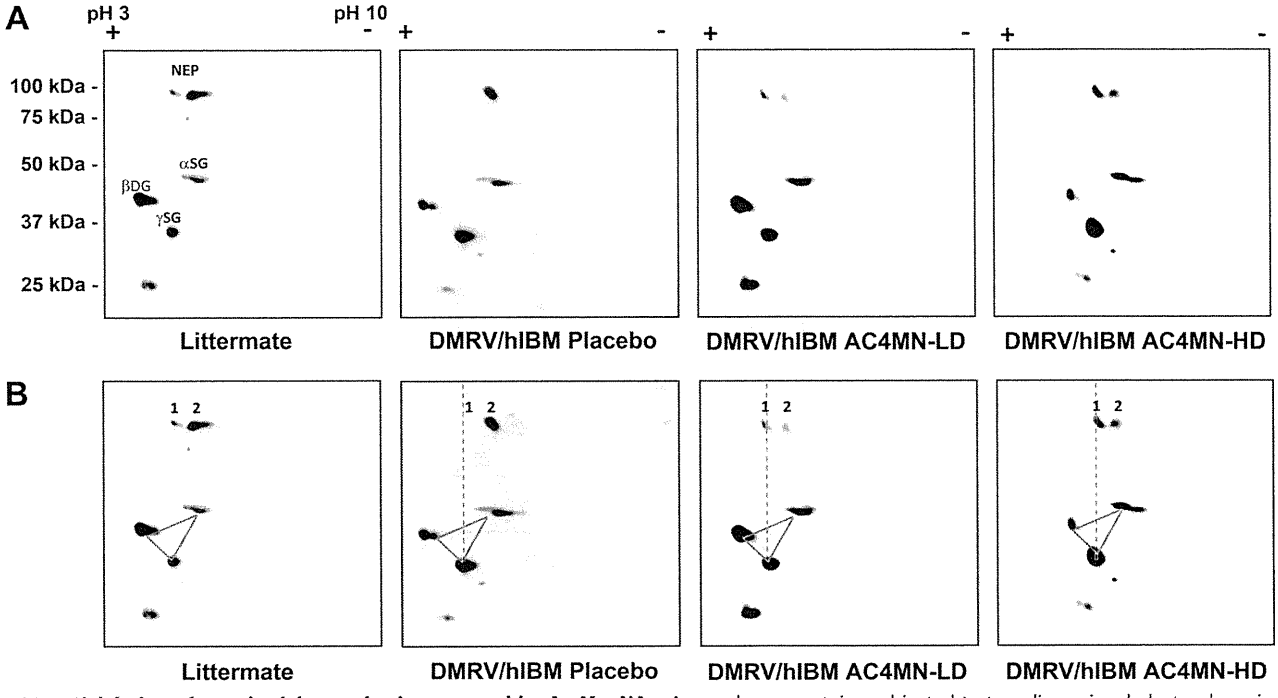

FIGURE 8. **Sialylation of muscle sialoproteins is recovered by Ac_4ManNAc.** *A*, membrane proteins subjected to two-dimensional electrophoresis and transferred to PVDF membrane are probed with known sialylated proteins: αSG, βDG, and NEP. γSG, a non-sialylated protein, was used as a control. The acidic end (pH 3) (+) is on the *left*, whereas the basic end (pH 10) (−) is on the *right* side of each membrane. Patterns are shown for control littermates without treatment and DMRV/hIBM mice (placebo, Ac4MN-LD, and Ac4MN-HD). *B*, duplicate image of *A* labeled to show the effect of treatment on the position of the identified proteins. Note the shift of αSG and βDG spots to the *right* in DMRV placebo as compared with littermate, indicating hyposialylation of proteins. After treatment, these spots are shifted to the *left*, indicating recovery of sialylation. For NEP, spot 1 is not detected in DMRV as compared with the littermate, and spot 2 is shifted toward the basic side. After treatment, spot 1 reappears, and spot 2 is shifted back to the *left* side.

at least among all ManNAc analogs, Ac_4ManNAc has been shown to be the least toxic (29). Although exogenously supplied Ac_4ManNAc in Jurkat cells was shown to induce apoptosis consequently leading to the conclusion that sialic acid metabolism may be involved in apoptosis (29), we did not find any toxic effects in mice when using this compound at least in the doses that were used. This might also be partly substantiated by the absence of altered morphology in tissue of mice that were given peracetylated *N*-propanoylmannosamine (41), an agent that was shown to exert higher cellular toxicity than Ac_4ManNAc (29).

Ac_5NeuAc, on the other hand, had effects similar to NeuAc in terms of increasing cellular sialylation, but when Ac_5NeuAc is esterified as in the case of Ac_5NeuAc-Me, this effect on sialylation is lost. Interestingly, Ac_5NeuAc-Me in addition to its failure to enhance cellular sialylation also induced cell death in DMRV myocytes even when smaller doses (compared with Ac_4ManNAc) are given, supporting the notion that the metabolic efficiency of a substrate is highly influenced by its effect on cell viability. The differences in the sialylation effect between Ac_5NeuAc and Ac_4ManNAc may be related to the pathway of incorporation of each compound into cells. ManNAc is incorporated into cells by passive diffusion directly across the plasma membrane, whereas NeuAc is incorporated into cells by macropinocytosis and then transported to the cytosol via the lysosomal system (42). Ac_5NeuAc may also be incorporated into the cell via same pathway as NeuAc, but it is then deacetylated within the lysosome.

Alternatively, the difference between Ac_5NeuAc and Ac_4ManNAc might be due to other factors. Although most enzymes in the sialic acid biosynthetic pathway are permissive to several substrates, some of the enzymes may exhibit substrate specificity. CMP synthetase, for example, was implicated to have some substrate specificity, probably depending on tissue or species specificity, as it allows the conversion of NeuAc, *N-glycolylneuraminic acid*, and 9-*O*-Ac-NeuAc but not 4-*O*-Ac-NeuAc to their respective CMP-sialic acid conjugates (43). In addition, the presence of specific sialyltransferases may influence the final incorporation of such substrates into glycoproteins (43). Another possibility is the activation of specific sialidases that can influence the final level of membrane-bound sialic acid. Further studies are needed to clarify this issue.

Pharmacokinetic profiles in mice showed the rapid excretion of administered Ac_4ManNAc into urine similar to ManNAc (19). Interestingly, the majority of administered Ac_4ManNAc in circulating blood and urine maintained its *O*-acetylation status, but when Ac_4ManNAc was incubated in serum at room temperature, almost all acetyl groups were released (data not shown), implying that prolonged exposure of Ac_4ManNAc in the serum without being mobilized for uptake by cells increases its vulnerability to the abundant esterases in the serum that can immediately degrade Ac_4ManNAc. These results suggest that to keep a considerable Ac_4ManNAc concentration in blood for therapeutic trials exogenous Ac_4ManNAc should be supplied continuously and frequently. The rapid excretion of Ac_4ManNAc might also

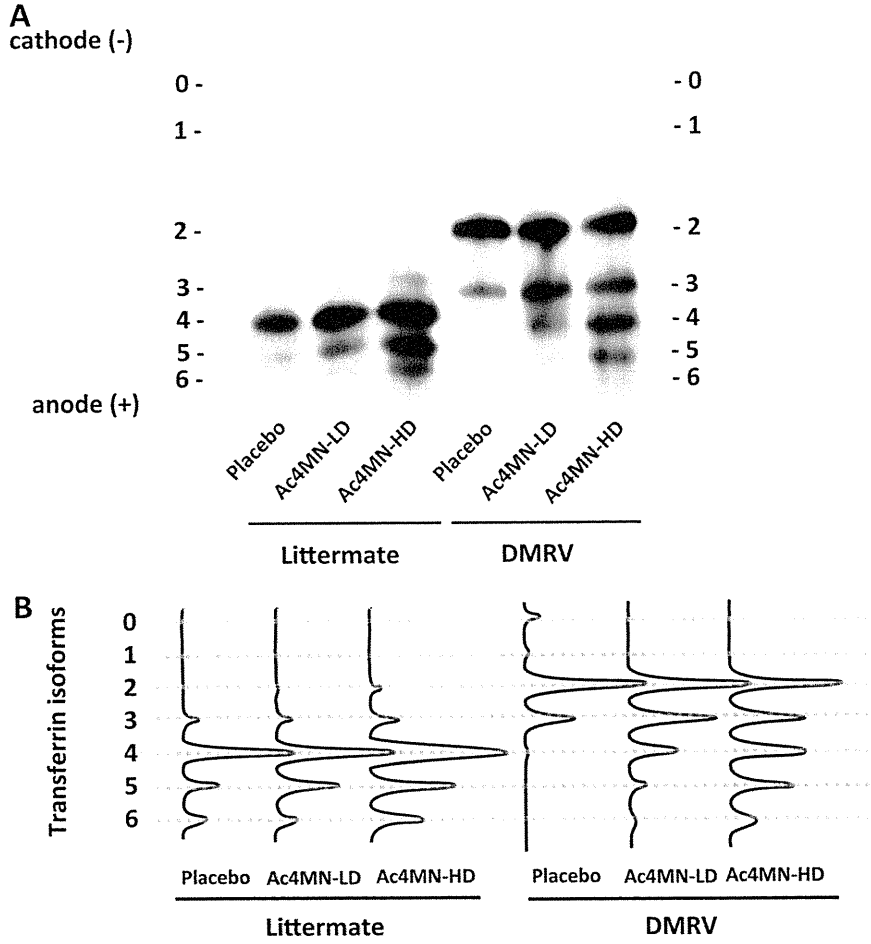

FIGURE 9. **Increase in sialylated forms of plasma transferrin in DMRV/hIBM mice is seen after treatment with Ac$_4$ManNAc.** *A*, iron-saturated plasma electrofocused in a 6% polyacrylamide gel that contained 10% ampholyte (pH 3–10), transferred to PVDF, and probed with anti-mouse transferrin demonstrates the electrophoretic profile of transferrin. Samples from control littermates and DMRV divided into three subgroups (placebo, Ac4MN-LD, and Ac4MN-HD) are shown. Six sialylated isoforms of transferrin are numbered *1–6* (*1*, monosialotransferrin; *2*, disialotransferrin; *3*, trisialotransferrin; *4*, tetrasialotransferrin, main isoform; *5*, pentasialotransferrin; *6*, hexasialotransferrin); asialotransferrin (*0*) is also indicated. In control littermates, isoforms 4 and 5 are readily visible, and after treatment, isoform 6 is observed along with the increase in isoforms 4 and 5. In non-treated DMRV (*P*) mice, isoforms 2 and 3 are seen as well as the asialotransferrin. After treatment, asialotransferrin disappears with increasing detection of isoforms 4, 5, and 6. *B*, the transferrin bands are quantified to show the changes in each isoform when comparing littermates and DMRV mice with or without treatment.

explain why it is relatively tolerated by mice *in vivo* despite its strong association with cell death by apoptosis *in vitro*. After a single administration of Ac$_4$ManNAc, about 16% is detected in the circulation (deduced from Fig. 2*A*) because of its rapid excretion. Unlike cells that do not have any route for excreting toxic substances, mice might have some regulating mechanisms that promote excretion of substances that are deemed toxic for survival, although this notion needs further studies for discussion.

The increase in tissue sialylation in Ac4MN-LD and Ac4MN-HD both in DMRV/hIBM mice and littermates provides further evidence that ManNAc analogs can be effectively incorporated in living organisms as has been shown by a previous study of the administration of *N*-propanoylmannosamine to wild type mice (41). After subcutaneous infusion of Ac$_4$ManNAc, however, a minimal effect was found in the intestine, indicating that the type of organ in which the sialic acid pool can be replenished may be influenced by the route of administration. As the changes in survival, motor performance, muscle size, function, and pathology were observed with increasing sialylation of tissues, especially of skeletal muscles, our present results further underscore the importance of addressing hyposialylation in understanding the mechanism of DMRV/hIBM.

In DMRV/hIBM mice, the degree of decline in the physiological properties of the skeletal muscles seemed to be correlated with the temporal feature of atrophy and weakness. In these mice, the P_t/CSA is reduced in middle age when intracellular inclusions that are mainly composed of amyloid were the most prominent feature, whereas there was parallel reduction of P_t/CSA and P_0/CSA during middle to older age (22). In this study, the gastrocnemius P_t/CSA of DMRV/hIBM mice in Ac4MN-LD were improved to levels almost comparable with those of littermates, but a complete recovery was seen only in Ac4MN-HD. In terms of P_0/CSA, the response in both treatment groups of DMRV/hIBM was similar to those in controls, implying that low dose Ac$_4$ManNAc is sufficient to improve P_0, which indicates the recovery of the contraction properties of

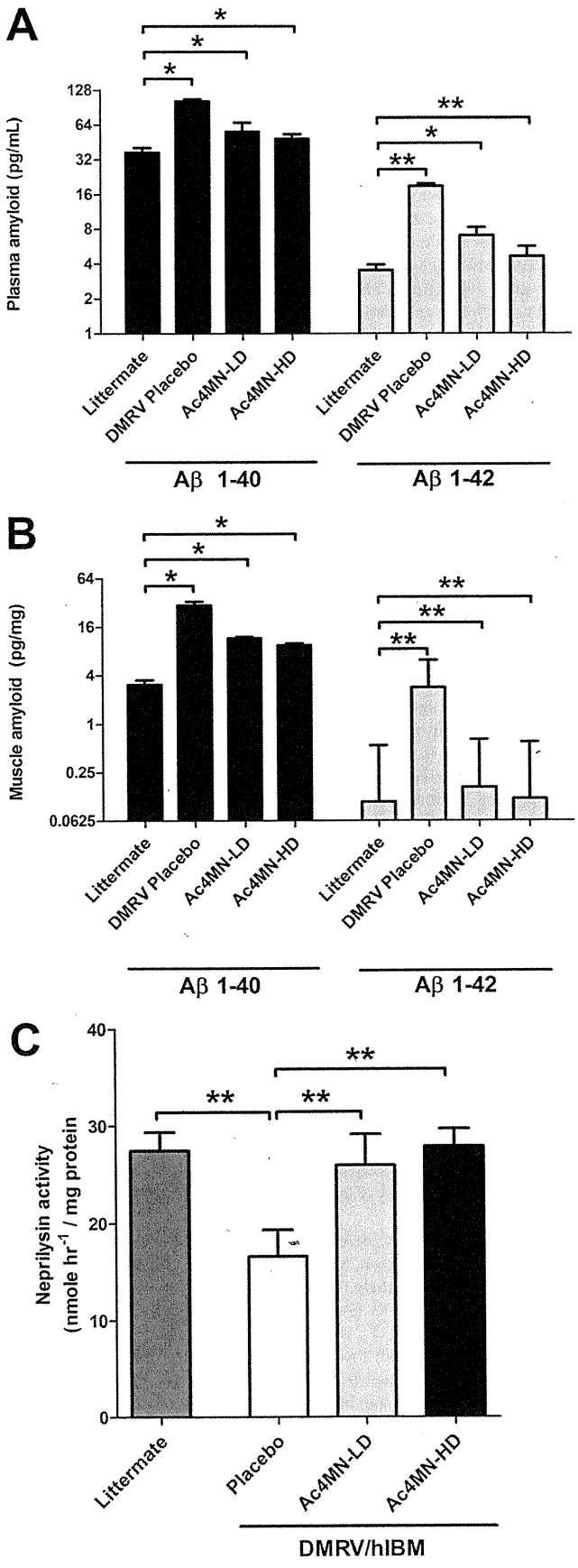

myofibrils. On the other hand, Ac4MN-HD showed complete recovery of muscle contraction systems, probably including other contraction machinery besides myofibrils. This may have some implication in deciding dosages in future endeavors.

Alterations in the sialylation status of glycoproteins in skeletal muscles from DMRV/hIBM patients have been reported. In certain muscle glycoproteins, including α-dystroglycan, increased reactivity to peanut agglutinin, a lectin that is reactive to desialylated forms of *O*-glycans, was observed (30); thus, it was proposed that the stability of such glycoproteins could be influenced by sialylation, and therefore these proteins could be involved in the pathomechanism of DMRV/hIBM. Likewise, it was also hypothesized that hyposialylation of neural cell adhesion molecule and NEP (26, 32) may contribute to the symptomatology of disease. In this study, we showed that hyposialylation of transferrin in blood, αSG and NEP in skeletal muscle, and podocalyxin in both kidney and skeletal muscles of DMRV/hIBM mouse were almost completely recovered after Ac_4ManNAc treatment, although until now, the relevance of changes in specific glycoproteins was still being clarified. However, hyposialylation of NEP, a catabolic enzyme for Aβ peptides, has been hypothesized to cause disturbance of amyloid metabolism at least in DMRV/hIBM (26). As amyloid deposits within myofibers precede the occurrence of rimmed vacuoles and muscle degeneration in DMRV/hIBM mice (18) and amyloid has been shown to exert toxicity in muscle cells (44), the NEP hypothesis may be a reasonable platform to explain the pathomechanism of DMRV/hIBM on the basis of hyposialylation and its effect on the progression of the disease. In this study, we demonstrated that NEP is hyposialylated and has reduced enzyme activity, and this occurs together with the increase in the amyloid burden within skeletal muscles in symptomatic DMRV/hIBM mice. Of note, Ac_4ManNAc treatment of DMRV/hIBM mice led to the recovery of NEP sialylation in addition to the normalization of NEP activity that may have contributed to the reduced amounts of Aβ peptides, consequently leading to normal functioning of the muscle. These findings suggest that the hyposialylation of NEP might be one of the factors in the increase in Aβ production in DMRV/hIBM myofibers that can possibly contribute to muscle degeneration. These results suggest the possibility that not only reduction of cellular sialylation but also the hyposialylation of certain glycoproteins, including transferrin, podocalyxin, and αSG, may be related to the pathomechanism of the disease in a manner that is yet to be elucidated. Nevertheless, these proteins may be used as biomarkers for future therapeutic trials in DMRV/hIBM.

FIGURE 10. **Increase in amyloid burden may be related to decreased NEP activity in DMRV/hIBM mice and is reversed by treatment with Ac_4ManNAc.** *A* and *B*, the amount of Aβ peptides 1–40 and 1–42 in the plasma (*A*) and skeletal muscle (*B*) are quantified by sandwich ELISA. Samples analyzed from control littermates and DMRV/hIBM (placebo, Ac4MN-LD, and Ac4MN-HD) are shown. *, $p < 0.05$; **, $p < 0.001$. *Error bars* represent standard S.E. *C*, analysis of NEP activity in total homogenates from skeletal muscles of littermates and DMRV/hIBM mice (placebo, Ac4MN-LD, and Ac4MN-HD). NEP activity is represented by the amount of *p*-nitroaniline released (nmol) in 1 h and normalized with the amount of protein homogenate (nmol/h/mg of protein). *Error bars* represent standard S.E.

In this study, we provide additional information on the proof of concept for sialic acid-related molecular therapy for DMRV/hIBM. The ideal monosaccharide should be one that can control metabolic flux in the sialic acid biosynthetic pathway in a time- and dose-dependent manner. In cells, Ac_4ManNAc has a very narrow concentration range (35), and its effect on cell sialylation is dependent on cell viability. But despite these findings, rapid excretion of Ac_4ManNAc in mice may allow incorporation of tolerable amounts into tissues, allowing cell viability and flux into the sialic acid pathway; this is eventually translated into increased sialylation in DMRV/hIBM tissues and modulation of the onset of symptoms. Application of this molecular therapy in trials involving DMRV/hIBM patients indeed will differ from other established pharmaceutical design mainly because of the extremely rapid excretion of sialic acid compounds and the need for long term administration. Nonetheless, the penultimate choice of monosaccharide would depend on careful analysis and consideration of the structure of the substrate, route and timing of administration, dose, and safety.

Acknowledgments—We thank Fumiko Funato for technical assistance. The monoclonal antibody (H4A3) that recognizes Lamp2, generated by J. T. August and James E. K. Hildreth, was obtained from the Development Studies Hybridoma Bank, developed under the auspices of the United States National Institute of Child Health and Human Development, National Institutes of Health and maintained by the University of Iowa, Department of Biological Sciences, Iowa City, IA.

REFERENCES

1. Nonaka, I., Noguchi, S., and Nishino, I. (2005) Distal myopathy with rimmed vacuoles and hereditary inclusion body myopathy. *Curr. Neurol. Neurosci. Rep.* **5,** 61–65
2. Nonaka, I., Sunohara, N., Ishiura, S., and Satoyoshi, E. (1981) Familial distal myopathy with rimmed vacuole and lamellar (myeloid) body formation. *J. Neurol. Sci.* **51,** 141–155
3. Argov, Z., and Yarom, R. (1984) "Rimmed vacuole myopathy" sparing the quadriceps. A unique disorder in Iranian Jews. *J. Neurol. Sci.* **64,** 33–43
4. Askanas, V., and Engel, W. K. (2003) in *The Molecular and Genetic Basis of Neurologic and Psychiatric Disease* (Rosenberg, R. N., Prusiner, S. B., DiMauro, S., Barchi, R. L., and Nestler, E. J., eds) 3rd Ed., pp. 501–509, Butterworth-Heinemann, Woburn, MA
5. Nishino, I., Malicdan, M. C., Murayama, K., Nonaka, I., Hayashi, Y. K., and Noguchi, S. (2005) Molecular pathomechanism of distal myopathy with rimmed vacuoles. *Acta Myol.* **24,** 80–83
6. Eisenberg, I., Avidan, N., Potikha, T., Hochner, H., Chen, M., Olender, T., Barash, M., Shemesh, M., Sadeh, M., Grabov-Nardini, G., Shmilevich, I., Friedmann, A., Karpati, G., Bradley, W. G., Baumbach, L., Lancet, D., Asher, E. B., Beckmann, J. S., Argov, Z., and Mitrani-Rosenbaum, S. (2001) The UDP-*N*-acetylglucosamine 2-epimerase/*N*-acetylmannosamine kinase gene is mutated in recessive hereditary inclusion body myopathy. *Nat. Genet.* **29,** 83–87
7. Kayashima, T., Matsuo, H., Satoh, A., Ohta, T., Yoshiura, K., Matsumoto, N., Nakane, Y., Niikawa, N., and Kishino, T. (2002) Nonaka myopathy is caused by mutations in the UDP-*N*-acetylglucosamine-2-epimerase/*N*-acetylmannosamine kinase gene (GNE). *J. Hum. Genet.* **47,** 77–79
8. Nishino, I., Noguchi, S., Murayama, K., Driss, A., Sugie, K., Oya, Y., Nagata, T., Chida, K., Takahashi, T., Takusa, Y., Ohi, T., Nishimiya, J., Sunohara, N., Ciafaloni, E., Kawai, M., Aoki, M., and Nonaka, I. (2002) Distal myopathy with rimmed vacuoles is allelic to hereditary inclusion body myopathy. *Neurology* **59,** 1689–1693
9. Stäsche, R., Hinderlich, S., Weise, C., Effertz, K., Lucka, L., Moormann, P., and Reutter, W. (1997) A bifunctional enzyme catalyzes the first two steps in *N*-acetylneuraminic acid biosynthesis of rat liver. Molecular cloning and functional expression of UDP-*N*-acetyl-glucosamine 2-epimerase/*N*-acetylmannosamine kinase. *J. Biol. Chem.* **272,** 24319–24324
10. Helenius, A., and Aebi, M. (2004) Roles of *N*-linked glycans in the endoplasmic reticulum. *Annu. Rev. Biochem.* **73,** 1019–1049
11. Iijima, R., Takahashi, H., Namme, R., Ikegami, S., and Yamazaki, M. (2004) Novel biological function of sialic acid (*N*-acetylneuraminic acid) as a hydrogen peroxide scavenger. *FEBS Lett.* **561,** 163–166
12. Wang, Z., Sun, Z., Li, A.V., and Yarema, K. J. (2006) Roles for UDP-GlcNAc 2-epimerase/ManNAc 6-kinase outside of sialic acid biosynthesis: modulation of sialyltransferase and BiP expression, GM3 and GD3 biosynthesis, proliferation, and apoptosis, and ERK1/2 phosphorylation. *J. Biol. Chem.* **281,** 27016–27028
13. Varki, N. M., and Varki, A. (2007) Diversity in cell surface sialic acid presentations: implications for biology and disease. *Lab. Invest.* **87,** 851–857
14. Keppler, O. T., Hinderlich, S., Langner, J., Schwartz-Albiez, R., Reutter, W., and Pawlita, M. (1999) UDP-GlcNAc 2-epimerase: a regulator of cell surface sialylation. *Science* **284,** 1372–1376
15. Schauer, R. (2004) Sialic acids: fascinating sugars in higher animals and man. *Zoology* **107,** 49–64
16. Noguchi, S., Keira, Y., Murayama, K., Ogawa, M., Fujita, M., Kawahara, G., Oya, Y., Imazawa, M., Goto, Y., Hayashi, Y. K., Nonaka, I., and Nishino, I. (2004) Reduction of UDP-*N*-acetylglucosamine 2-epimerase/*N*-acetylmannosamine kinase activity and sialylation in distal myopathy with rimmed vacuoles. *J. Biol. Chem.* **279,** 11402–11407
17. Hinderlich, S., Salama, I., Eisenberg, I., Potikha, T., Mantey, L. R., Yarema, K. J., Horstkorte, R., Argov, Z., Sadeh, M., Reutter, W., and Mitrani-Rosenbaum, S. (2004) The homozygous M712T mutation of UDP-*N*-acetylglucosamine 2-epimerase/*N*-acetylmannosamine kinase results in reduced enzyme activities but not in altered overall cellular sialylation in hereditary inclusion body myopathy. *FEBS Lett.* **566,** 105–109
18. Malicdan, M. C., Noguchi, S., Nonaka, I., Hayashi, Y. K., and Nishino, I. (2007) A Gne knockout mouse expressing human GNE D176V mutation develops features similar to distal myopathy with rimmed vacuoles or hereditary inclusion body myopathy. *Hum. Mol. Genet.* **16,** 2669–2682
19. Malicdan, M. C., Noguchi, S., Hayashi, Y. K., Nonaka, I., and Nishino, I. (2009) Prophylactic treatment with sialic acid metabolites precludes the development of the myopathic phenotype in the DMRV-hIBM mouse model. *Nat. Med.* **15,** 690–695
20. Malicdan, M. C., Noguchi, S., and Nishino, I. (2009) Monitoring autophagy in muscle diseases. *Methods Enzymol.* **453,** 379–396
21. Hara, S., Yamaguchi, M., Takemori, Y., Furuhata, K., Ogura, H., and Nakamura, M. (1989) Determination of mono-*O*-acetylated *N*-acetylneuraminic acids in human and rat sera by fluorometric high-performance liquid chromatography. *Anal. Biochem.* **179,** 162–166
22. Malicdan, M. C., Noguchi, S., Hayashi, Y. K., and Nishino, I. (2008) Muscle weakness correlates with muscle atrophy and precedes the development of inclusion body or rimmed vacuoles in the mouse model of DMRV/hIBM. *Physiol. Genomics* **35,** 106–115
23. Yamamoto, H., Hagiwara, Y., Mizuno, Y., Yoshida, M., and Ozawa, E. (1993) Heterogeneity of dystrophin-associated proteins. *J. Biochem.* **114,** 132–139
24. Kim, S., Westphal, V., Srikrishna, G., Mehta, D. P., Peterson, S., Filiano, J., Karnes, P. S., Patterson, M. C., and Freeze, H. H. (2000) Dolichol phosphate mannose synthase (DPM1) mutations define congenital disorder of glycosylation Ie (CDG-Ie) *J. Clin. Investig.* **105,** 191–198
25. Hackler, R., Arndt, T., Helwig-Rolig, A., Kropf, J., Steinmetz, A., and Schaefer, J. R. (2000) Investigation by isoelectric focusing of the initial carbohydrate-deficient transferrin (CDT) and non-CDT transferrin isoform fractionation step involved in determination of CDT by the ChronAlcol.D. assay. *Clin. Chem.* **46,** 483–492
26. Broccolini, A., Gidaro, T., De Cristofaro, R., Morosetti, R., Gliubizzi, C., Ricci, E., Tonali, P. A., and Mirabella, M. (2008) Hyposialylation of neprilysin possibly affects its expression and enzymatic activity in hereditary inclusion-body myopathy muscle. *J. Neurochem.* **105,** 971–981
27. Thompson, M. W., Govindaswami, M., and Hersh, L. B. (2003) Mutation of active site residues of the puromycin-sensitive aminopeptidase: conver-

sion of the enzyme into a catalytically inactive binding protein. *Arch. Biochem. Biophys.* **413,** 236–242
28. Liu, Y., Studzinski, C., Beckett, T., Guan, H., Hersh, M. A., Murphy, M. P., Klein, R., and Hersh, L. B. (2009) Expression of neprilysin in skeletal muscle reduces amyloid burden in a transgenic mouse model of Alzheimer disease. *Mol. Ther.* **17,** 1381–1386
29. Kim, E. J., Sampathkumar, S. G., Jones, M. B., Rhee, J. K., Baskaran, G., Goon, S., and Yarema, K. J. (2004) Characterization of the metabolic flux and apoptotic effects of *O*-hydroxyl- and *N*-acyl-modified *N*-acetylmannosamine analogs in Jurkat cells. *J. Biol. Chem.* **279,** 18342–18352
30. Tajima, Y., Uyama, E., Go, S., Sato, C., Tao, N., Kotani, M., Hino, H., Suzuki, A., Sanai, Y., Kitajima, K., and Sakuraba, H. (2005) Distal myopathy with rimmed vacuoles: impaired *O*-glycan formation in muscular glycoproteins. *Am. J. Pathol.* **166,** 1121–1130
31. Huizing, M., Rakocevic, G., Sparks, S. E., Mamali, I., Shatunov, A., Goldfarb, L., Krasnewich, D., Gahl, W. A., and Dalakas, M. C. (2004) Hypoglycosylation of α-dystroglycan in patients with hereditary IBM due to GNE mutations. *Mol. Genet. Metab.* **81,** 196–202
32. Galeano, B., Klootwijk, R., Manoli, I., Sun, M., Ciccone, C., Darvish, D., Starost, M. F., Zerfas, P. M., Hoffmann, V. J., Hoogstraten-Miller, S., Krasnewich, D. M., Gahl, W. A., and Huizing, M. (2007) Mutation in the key enzyme of sialic acid biosynthesis causes severe glomerular proteinuria and is rescued by *N*-acetylmannosamine. *J. Clin. Investig.* **117,** 1585–1594
33. Vattemi, G., Engel, W. K., McFerrin, J., Pastorino, L., Buxbaum, J. D., and Askanas, V. (2003) BACE1 and BACE2 in pathologic and normal human muscle. *Exp. Neurol.* **179,** 150–158
34. Jacobs, C. L., Goon, S., Yarema, K. J., Hinderlich, S., Hang, H. C., Chai, D. H., and Bertozzi, C. R. (2001) Substrate specificity of the sialic acid biosynthetic pathway. *Biochemistry* **40,** 12864–12874
35. Jones, M. B., Teng, H., Rhee, J. K., Lahar, N., Baskaran, G., and Yarema, K. J. (2004) Characterization of the cellular uptake and metabolic conversion of acetylated *N*-acetylmannosamine (ManNAc) analogues to sialic acids. *Bioteclmol. Bioeng.* **85,** 394–405
36. Viswanathan, K., Lawrence, S., Hinderlich, S., Yarema, K. J., Lee, Y. C., and Betenbaugh, M. J. (2003) Engineering sialic acid synthetic ability into insect cells: identifying metabolic bottlenecks and devising strategies to overcome them. *Biochemistry* **42,** 15215–15225
37. Collins, B. E., Fralich, T. J., Itonori, S., Ichikawa, Y., and Schnaar, R. (2000) Conversion of cellular sialic acid expression from *N*-acetyl- to *N*-glycolylneuraminic acid using a synthetic precursor, *N*-glycolylmannosamine pentaacetate: inhibition of myelin-associated glycoprotein binding to neural cells. *Glycobiology* **10,** 11–20
38. Yarema, K. J. (2001) New directions in carbohydrate engineering: a metabolic substrate-based approach to modify the cell surface display of sialic acids. *BioTechniques* **31,** 384–393
39. Sarkar, A. K., Rostand, K. S., Jain, R. K., Matta, K. L., and Esko, J. D. (1997) Fucosylation of disaccharide precursors of sialyl LewisX inhibit selectin-mediated cell adhesion. *J. Biol. Chem.* **272,** 25608–25616
40. Keppler, O. T., Horstkorte, R., Pawlita, M., Schmidt, C., and Reutter, W. (2001) Biochemical engineering of the *N*-acyl side chain of sialic acid: biological implications. *Glycobiology* **11,** 11R–18R
41. Gagiannis, D., Gossrau, R., Reutter, W., Zimmermann-Kordmann, M., and Horstkorte, R. (2007) Engineering the sialic acid in organs of mice using *N*-propanoylmannosamine. *Biochim. Biophys. Acta* **1770,** 297–306
42. Bardor, M., Nguyen, D. H., Diaz, S., and Varki, A. (2005) Mechanism of uptake and incorporation of the non-human sialic acid *N*-glycolylneuraminic acid into human cells. *J. Biol. Chem.* **280,** 4228–4237
43. Higa, H. H., and Paulson, J. C. (1985) Sialylation of glycoprotein oligosaccharides with *N*-acetyl-, *N*-glycolyl-, and *N*-*O*-diacetylneuraminic acids. *J. Biol. Chem.* **260,** 8838–8849
44. Querfurth, H. W., Suhara, T., Rosen, K. M., McPhie, D. L., Fujio, Y., Tejada, G., Neve, R. L., Adelman, L. S., and Walsh, K. (2001) β-Amyloid peptide expression is sufficient for myotube death: implications for human inclusion body myopathy. *Mol. Cell. Neurosci.* **17,** 793–810

Neuroscience Research 72 (2012) 181–186

Contents lists available at SciVerse ScienceDirect

Neuroscience Research

journal homepage: www.elsevier.com/locate/neures

Continuous administration of poloxamer 188 reduces overload-induced muscular atrophy in dysferlin-deficient SJL mice

Naoki Suzuki[a,*], Tetsuya Akiyama[a], Toshiaki Takahashi[b], Hazuki Komuro[a], Hitoshi Warita[a], Maki Tateyama[a], Yasuto Itoyama[c], Masashi Aoki[a]

[a] Department of Neurology, Tohoku University School of Medicine, 1-1 Seiryo-machi, Aoba-ku, Sendai, Japan
[b] Department of Neurology, National Nishitaga Hospital, Sendai, Japan
[c] National Center Hospital, National Center of Neurology and Psychiatry (NCNP), Tokyo, Japan

ARTICLE INFO

Article history:
Received 28 May 2011
Received in revised form 3 October 2011
Accepted 4 October 2011
Available online 21 October 2011

Keywords:
Dysferlinopathy
Muscular dystrophy
Poloxamer 188 (P188)
Osmotic pump
p38
Atrogin-1

ABSTRACT

Dysferlin-deficient SJL mice are commonly used to study dysferlinopathy. We demonstrated that poloxamer 188 (P188), a membrane sealant, is effective in reducing the loss of muscle mass in SJL mice when administered using an osmotic pump for 6 weeks. We did not observe significant changes over a 2-week administration period, suggesting that longthier observation is necessary to determine the effectiveness of P188. We also examined exercise endurance in P188-administered SJL mice using a rolling cage. Phosphorylated p38 was found to be reduced in P188-administered SJL mice; additionally, using microarray analysis, we found diminished expression of atrogin-1, an E3 ubiquitin ligase, as the effector of muscular atrophy. Chronic infusion of P188 to dysferlin-deficient SJL mice reduced muscular atrophy, and administering p38 and atrogin-1 in the gastrocnemius muscle improved its motor function. These results provide a basis for potential treatments for dysferlin-deficient skeletal muscle fibers.

1. Introduction

Mutations in the dysferlin gene cause several phenotypes of muscular dystrophy, called "dysferlinopathies"; these include limb-girdle muscular dystrophy type 2B (LGMD2B), Miyoshi myopathy (MM), and distal anterior compartment myopathy (DACM) (Aoki et al., 2001; Bashir et al., 1998; Illa et al., 2001; Klinge et al., 2010; Liu et al., 1998; Paradas et al., 2010; Rosales et al., 2010; Takahashi et al., 2003). Dysferlinopathies are autosomal recessive diseases, and different phenotypes are observed even within the same family (Illarioshkin et al., 2000; Saito et al., 2007). Dysferlin deficiency has been proven to lead to defective membrane resealing in skeletal muscle and muscle necrosis (Bansal et al., 2003).

SJL mice, which display dysferlin deficiencies (Bittner et al., 1999) and inflammatory muscle changes (Suzuki et al., 2005), are commonly used to study dysferlinopathy. The spontaneous myopathy of SJL mice begins at 4–6 weeks of age and is nearly complete by eight months of age. The mutation in SJL mice is an in-frame deletion of 171 base pairs of the dysferlin gene. Assuming that the structure of the gene is similar in mice and humans, this in-frame deletion predicts that in human mutations 57 amino acids of dysferlin protein, including most of the fourth C2 domain, would be absent.

Poloxamer 188 (P188) is a stable 8.4 kDa amphiphilic polymer that localizes in lipid monolayers (Wu et al., 2005) and damaged regions of membranes (Maskarinec et al., 2005). When applied to injured cells, P188 repairs disrupted membranes and enhances the recovery of skeletal muscle (Lee et al., 1992), fibroblasts (Merchant et al., 1998), and the spinal cord (Borgens et al., 2004) following a variety of injury-inducing protocols. Chemically based membrane sealants have been acutely tested in mdx mice and have recently been proposed as a new therapeutic approach for cardiac membrane stabilization in muscular dystrophy (Yasuda et al., 2005). This treatment modality aims to directly seal the membrane tears that occur in the absence of dystrophin. Cases of Duchenne muscular dystrophy (DMD) in mdx mice showed that application of the membrane sealant poloxamer 188 (P188) confers acute cardiac protection. Additionally, the chronic infusion of severely affected dystrophic dogs with membrane-sealing poloxamer reduced myocardial fibrosis and fully prevented left ventricular remodeling (Townsend et al., 2010). The effects of P188 on other types of muscular dystrophy have not been examined.

Our aim was to determine the effects of P188 when administered with an osmotic pump for 6 weeks in a mouse model of dysferlinopathy. Using SJL mice, we found that p38 and atrogin-1 played

* Corresponding author. Tel.: +81 22 717 7189; fax: +81 22 717 7192.
E-mail address: naoki@med.tohoku.ac.jp (N. Suzuki).

0168-0102/$ – see front matter © 2011 Elsevier Ireland Ltd and the Japan Neuroscience Society. All rights reserved.
doi:10.1016/j.neures.2011.10.005

key roles in the influence of P188 on the progression of muscular atrophy induced by overloading.

2. Materials and methods

2.1. Animals

All mice were handled according to approved animal protocols in our institution. Gastrocnemius and tibialis anterior muscles were dissected from female control mice (SWR) and SJL (SJL/JOrllcoCrj) mice (Charles River Japan Inc., Yokohama, Japan) ($n = 10$ and 50, respectively). Prior to this study, we had examined the muscles of both strains of mice to investigate the muscular pathology and progression of myopathy (Suzuki et al., 2005). In 2-month-old SJL mice, there were slight or no muscle changes compared with the control mice. In contrast, 9-month-old SJL mice had an increased variety of fiber diameters, degenerating fibers, regenerating fibers, and increased inflammatory responses. With those results in mind, mice within the 19- to 25-week age range were chosen for use.

2.2. Creatine kinase (CK) determination

Blood (200 μL) was collected in Eppendorf tubes using cardiac puncture under deep anesthesia and allowed to clot at room temperature prior to centrifugation and serum collection. CK determination was performed according to the manufacturer's instructions using a standard spectrophotometric method. The data were expressed as units per liter.

2.3. Reagents and osmotic pump

19-Week-old mice were operated upon. Sterile saline was injected into the control mice. The total dose of poloxamer 188 (P188; Sigma–Aldrich, MO) was 20 mg, infused continuously for 42 days. The dosage was modified from that used in previous reports (Ng et al., 2008; Quinlan et al., 2006; Yasuda et al., 2005). The osmotic pumps (Alzet osmotic pump 2006, Alzet, CA) were incubated in sterile saline at 37 °C for 40 h to attain a constant flow rate prior to use. The pumps were filled to capacity with either P188 or sterile saline using a filling needle. SJL and SWR mice (19 weeks old) were anesthetized using intraperitoneal Nembutal. The skin between the scapulas was incised, and the pumps were implanted in the subcutaneous pocket. The normal pumping rate was 0.15 μL/h for 6 weeks. The reservoir volume was 200 μL, and the weight of each osmotic pump was 1.1 g. The mice were sampled at 25 weeks old, with body weights between 25 and 30 g.

2.4. Functional tests

Grip strength of the forearms was assessed using a grip strength meter (GPM-100, MelQuest, Japan) according to the manufacturer's instructions. 25-Week-old mice were used. Three successful forelimb strength measurements ($n = 5$) were recorded in the morning by an investigator blinded to treatment conditions. The average grip strength measurement from each day was used for the subsequent analysis. Motor endurance was measured using a rolling cage (RS-204-5, Kori-Seiki, Japan). The number of rotations per day was recorded, and the average number of rotations for three consecutive days was calculated ($n = 5$).

2.5. Tissue preparation

Both body and wet muscle weight were recorded. The gastrocnemius and tibialis anterior muscles were collected individually using standard dissection methods and cleaned of excess fat, connective tissue, and tendons. Several of the muscles were frozen in isopentane that was cooled by liquid nitrogen for histological and immunohistochemical analysis, whereas the other muscles were frozen directly in liquid nitrogen for either RNA isolation or protein extraction and stored at −80 C.

2.6. RNA extraction

RNA was extracted from the gastrocnemius, tibialis anterior, and soleus muscles using Qiagen RNeasy Fibrous Tissue Mini Kits (Qiagen, CA). RNA concentrations were determined using a spectrophotometer, and the RNA quality was assessed using an Agilent 2100 Bioanalyzer (Agilent Technologies, CA). All RNA samples had RNA Integrity Numbers (RIN) of 9.0 or higher.

2.7. Real time PCR

For RT-PCR, first strand cDNA was synthesized using oligo-dT primers. The expression levels of selected genes (atrogin-1/MAFbx and beta-actin) were analyzed using CFX96 (BioRad, CA) following the manufacturer's instructions. The primers were 5′-TCGCAGCCAAGAAGAGAAAG-3′, 5′-GGCAGTCGAGAAGTCCAGTC-3′ for atrogin-1 and 5′-CTGGCTCCTAGCACCATGAAGAT-3′, 5′-GGTGGACAGTGAGGCCAGGAT-3′ for beta-actin.

2.8. Western blotting

Skeletal muscle protein was extracted from mouse hindlimb muscle samples for Western blot analysis. We used the Bradford method and Coomassie Brilliant Blue G-250 (Bio-Rad) to determine the protein concentrations. Protein fractions were then extracted using a reducing sample buffer containing 10% SDS, 70 mM Tris–HCl, 5% β-mercaptoethanol and complete inhibitor cocktail (Roche, Basel, Swiss). Protein (15 or 30 μg per lane) was separated on a SDS-polyacrylamide gel, and the resulting gel was subsequently transferred to a polyvinylidene difluoride membrane (Millipore) using 250 mA for 1 h. The blot was later incubated with the primary antibodies. The signals were detected using the enhanced chemiluminescence plus method (GE, NJ). Relative quantities of proteins in the western blots were determined using scanning densitometry and expressed in arbitrary units.

2.9. Nuclear fractionation

2.9.1. Nuclear and cytosolic protein extraction

Nuclear extracts were taken from mouse skeletal muscle as previously described (Suzuki et al., 2007). The cytosolic extract was obtained from the first supernatant of the nuclear extract preparation. The supernatant was placed in Millipore Ultrafree-4 centrifugal columns that had been pre-wetted with 0.5 mL of dilution buffer (20 mM HEPES, 40 mM KCl, 10% glycerol, 0.2 mM EDTA, 1 mM DTT) and centrifuged (7500 × g) at 4 °C for 30 min. Dilution buffer (0.8 mL) was added to the column, and the 30-min spin was repeated.

2.10. Statistical analysis

Significant differences were determined with either the unpaired Student's t-test or the Mann–Whitney test using Excel. All data are expressed as the means ± SEM. Statistical significance is defined as $^{*}p < 0.05$.

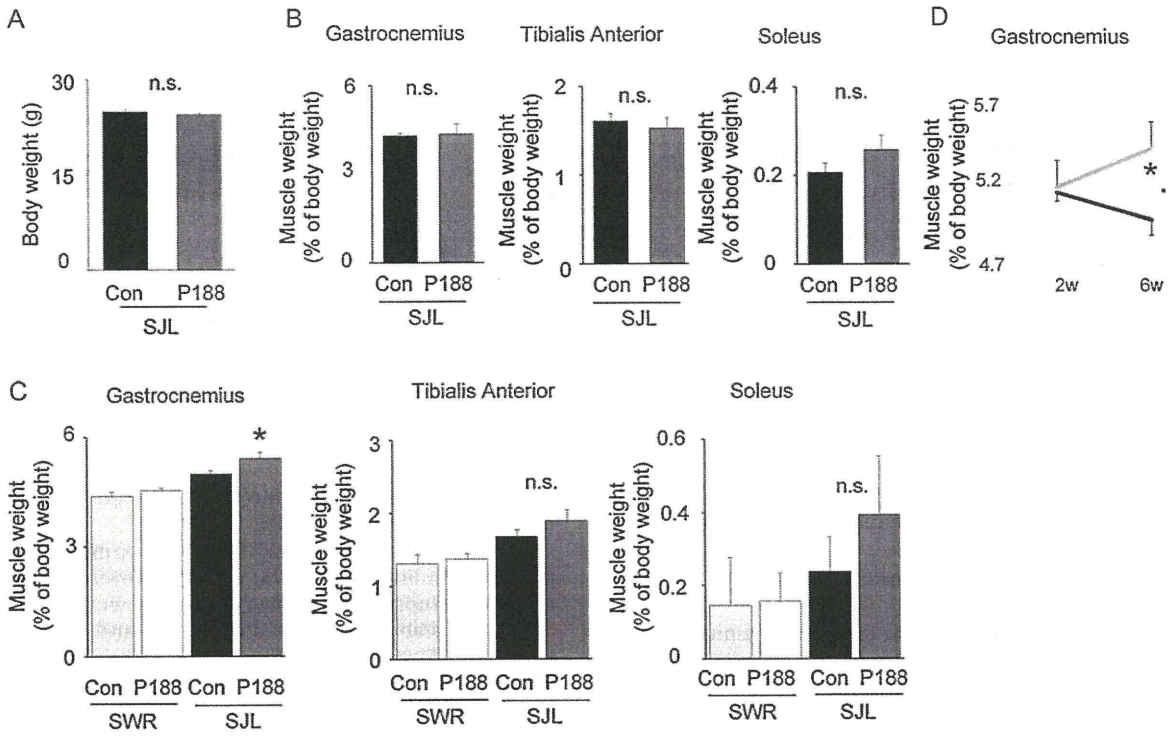

Fig. 1. Muscle mass loss is alleviated in P188-administered SJL mice. (A) Body mass in saline- (control: Con) and P188-administered SJL mice ($n = 10$ per group). n.s., not significant. Student's t-test, $^*p < 0.05$. (B and C) Gastrocnemius, tibialis anterior, and soleus muscles: mass from control group and P188-administered SJL mice ($n = 10$ per group) after 2 weeks (B) and 6 weeks (C). SWR mice were also examined as a control. (D) Transitional changes in muscle mass of gastrocnemius muscle from 2 to 6 weeks after the start of administration of saline and P188 in SJL mice. n.s., not significant. Student's t-test, $^*p < 0.05$.

3. Results

3.1. P188 inhibits the decline of muscle mass in osmotic pump-implanted SJL mice

The body weights of saline- (control: Con) and P188-administered SJL mice ($n = 10$ per group) did not change significantly during the 6-week experimental period (Fig. 1A). The muscle masses of saline- and P188-administered mice did not change during the first 2 weeks (Fig. 1B); however, the gastrocnemius muscles of the saline-administered mice had decreased in mass after 6 weeks. Gastrocnemius mass in the P188-administered mice, in contrast, seemed to increase significantly during those 6 weeks (Fig. 1C and D), suggesting that muscular atrophy was suppressed by P188. Compared to the SWR mice, the SJL mice muscle display several unique features including fibrosis, fiber degeneration and inflammatory cell infiltration (Suzuki et al., 2005). It has also been reported that their muscle is generally greater in mass than that of C57BL6 mice's muscle (Rayavarapu et al., 2010). In our study the SJL mice's muscle mass was greater than that of SWR mice, so we next examined the functional status of P188-administered SJL mice. We found, on average, significantly increased muscle fiber in a cross-sectional area (Supplementary Fig. 1). The forearm grip strength had not changed among saline- and P188-administered SJL mice (Fig. 2A); however, rolling cage observation revealed significantly greater running endurance in P188-administered SJL mice

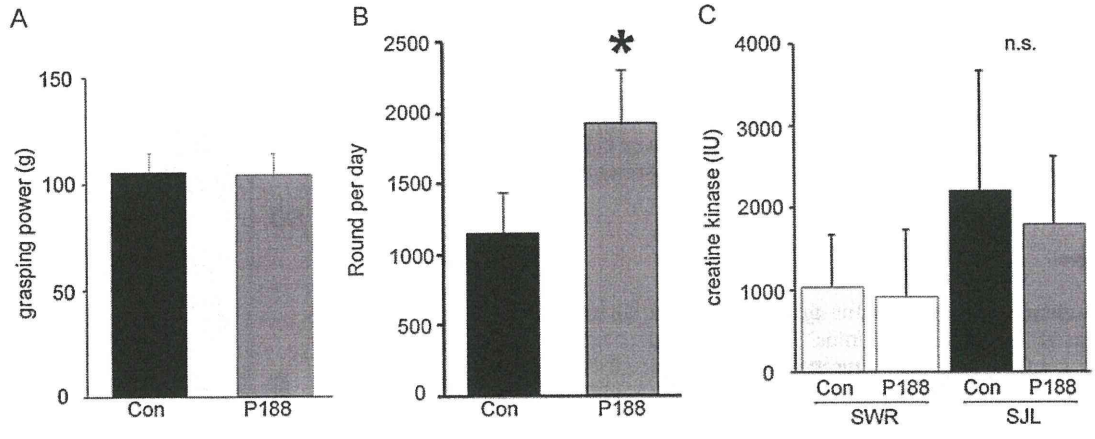

Fig. 2. P188 improves motor function in SJL mice. (A) Grip strength is not different among saline- (control: Con) and P188-administered SJL mice ($n = 10$ per group). (B) Rolling cage observation revealed greater running function in P188-administered SJL mice ($n = 10$ per group). Student's t-test, $^*p < 0.05$. (C) P188 did not reduce serum CK in SJL mice. SWR mice were also examined as a control.

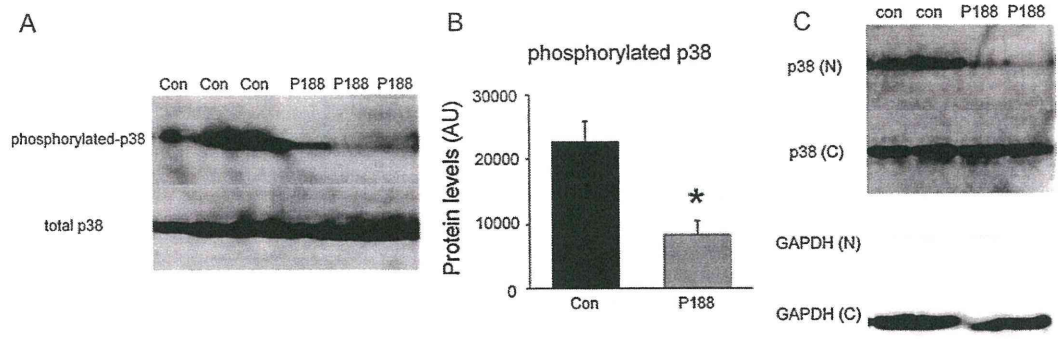

Fig. 3. Phosphorylation and localization of p38 is controlled by P188 administration. (A) Representative immunoblot analysis for p38 and phosphorylated p38 in saline- (Con) and P188-administered SJL mice. (B) The amount of phosphorylated p38 in saline- (Con) and P188-administered SJL mice. (C) Representative immunoblot analysis for nuclear (N) and cytoplasmic (C) p38 and GAPDH (as a technical control).

than in saline-administered SJL mice (Fig. 2B). P188 did not significantly reduce serum CK levels in SJL mice (Fig. 2C).

3.2. *Effect of P188 is through a p38-mediated pathway*

We found reduced muscle loss in the gastrocnemius muscles of P188-administered SJL mice and increased exercise capability in the rolling cage. Next, we examined the molecular mechanism of P188's effects on muscle mass. We first examined the membrane repair mechanism using Evans blue dye (Supplementary Fig. S2) because P188 is a membrane-sealing reagent. We did not find significant differences between saline- and P188-administered SJL mice in the Evans Blue-positive muscle fibers. We also examined the rate of apoptosis in the gastrocnemius muscles (Supplementary Fig. S3) and Mac1-positive infiltrated cells (Supplementary Fig. S4), but found no significant difference between the saline- and P188-administered SJL mice.

We then examined the molecular pathway of muscular atrophy in the gastrocnemius muscle. We found reduced phosphorylated p38 in P188-administered SJL mice compared with saline-administered mice (Fig. 3A and B), as well as decreased p38 in the nuclear fraction of the gastrocnemius muscle homogenate (Fig. 3C). We also found that basal levels of p38 are low in both untreated and P188-treated wild-type mice (Supplementary Fig. S5), suggesting that the increased levels of p38 are related to the pathophysiology of SJL mice. We observed that Foxo3a, pFoxo3a, Akt, pAkt, p65, acetyl-p65, nitric oxide synthase (NOS) and the chief components of the dystrophin glycoprotein complex had not changed (Supplementary Fig. S6).

To examine the downstream events of P188 administration, we performed a microarray analysis of saline- and P188-administered SJL mice (Supplementary Table 1). We found significantly reduced expression of atrogin-1, which is an E3 ubiquitin ligase in skeletal muscle. MuRF-1 did not change significantly in the microarray analysis (data not shown). We confirmed that atrogin-1 was significantly lower in the P188-administered SJL mice by real-time PCR (Fig. 4).

4. Discussion

We have demonstrated that adult dysferlin-deficient SJL mice show decreased loss of gastrocnemius muscle and higher activity levels in a rolling cage following the administration of P188 through an osmotic pump for 6 weeks. The grip strength did not vary between saline- and P188-administered mice, as instantaneous muscle strength may not be affected in a chronic model. We also reported the amount of decrease in phosphorylated and intranuclear p38 protein following the continuous administration of P188. Furthermore, the expression of atrogin-1 was suppressed in P188-administered SJL mice.

Previous studies have established P188 as a membrane-patching polymer that interacts directly with monolayers (Wu et al., 2005) and the disrupted membrane (Maskarinec et al., 2005). P188 is effective in stabilizing membranes and enhances the recovery of a variety of cell types following an array of injury-inducing protocols (Borgens et al., 2004; Lee et al., 1992; Merchant et al., 1998; Yasuda et al., 2005); however, we found no significant changes using Evans blue dye staining. Because the sensitivity of EBD is not especially high, however, further membrane-repairing experiments (Bansal et al., 2003) are necessary to determine whether the membrane has recovered.

p38 affects the activities of transcription factors from the MyoD and MEF2 families and participates in the remodeling of chromatin at specific muscle-regulatory regions. p38 also has a crucial role in development and differentiation (Keren et al., 2006). Doxorubicin, an anti-tumor agent of the anthracycline family and a cardiotoxic drug, induces atrogin-1 through a p38-MAPK-dependent pathway in cardiac myocytes (Yamamoto et al., 2008). P188 was also reported to inhibit apoptosis and prevent necrosis of the pheochromocytoma cell line following mechanical trauma by inhibiting p38 (Serbest et al., 2006). The activation of p38 MAPK phosphorylation occurs as soon as 8 h after lipopolysaccharide injection into the skeletal muscles of mice, as well as in C2C12 myotubes with oxidant hydrogen peroxide. The inhibition of p38 by SB202190 prevented peroxide-induced atrophy, with diminished upregulation of atrogin-1 and MuRF-1 (McClung et al., 2010). These data suggest that p38 may be a mediator of the ubiquitin proteasome system,

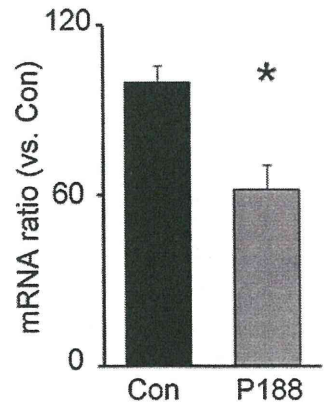

Fig. 4. Semi-quantitative PCR for genes differently expressed in a microarray assay. (A) mRNA levels of atrogin-1/MAFbx ($n = 5$) in gastrocnemius muscle from saline- (Con) and P188-administered SJL mice ($^*p < 0.05$, Mann–Whitney test).

regulated by poloxamer 188 in our model. Compared with the SWR mice shown in supplementary Fig. 5, p38 is upregulated only in dysferlin-deficient SJL mice. The upregulated p38 is suppressed in SJL mice by P188, so we speculated that P188 may inhibit the dysferlin-deficiency induced p38-atrogin1-muscle atrophy pathway in SJL mice. Pathways other than p38-atrogin1 should also be examined as the downstream target of poloxamer 188.

Poloxamer 188, previously named RheothRx, significantly reduced total analgesic use, pain intensity and total days of hospitalization in human patients with moderate to severe vasoocclusive episodes (Adams-Graves et al., 1997). Poloxamer 188 was well tolerated in humans; there was no significant difference between treatment and placebo groups in terms of adverse experience. As shown in Figs. 1 and 2, P188 had no effect on muscle mass in wild-type mice. Yasuda et al. (2005) also reported that P188 has no effect on left ventricular end-diastolic volumes immediately following the infusion of P188 in control mice. Thus, we concluded that the effects of P188 on wild-type mice are minimal, if they exist at all. Poloxamer 188 administered to animals decreased myocyte injury, preserved adenosine 5′-triphosphate levels in the tissue, and improved survival following hind limb ischemia-reperfusion injury (Murphy et al., 2010). As proposed by Townsend et al. (2010), long-term administration of P188 maintains the myocardial membrane function and prevents myocardial necrosis. Our results also suggest that poloxamer 188, which has been approved by the U.S. Food and Drug Administration for other uses, could become a beneficial clinical option as a late salvage therapy.

The beneficial effects of long-term application of P188 to the skeletal muscles of SJL mice were detected in this study. The SJL mice presented a loss of muscle mass after 6 weeks of observation due to the extra weight of the infusion pump and solutions; these factors would be expected to increase the frequency of mechanically induced disruptions of membrane integrity, which are important events in the pathophysiology of dysferlin deficiency in skeletal muscle. This accelerated disease progression makes the protective effects of P188 even more notable.

Using an osmotic pump for continuous administration, we demonstrated for the first time that P188, a membrane-sealing poloxamer, is effective in reducing loss of gastrocnemius muscle mass and increasing exercise endurance. These results provide the basis for potential therapeutic strategies utilizing P188 and the p38-mediated pathway in dysferlin-deficient skeletal muscles.

Acknowledgements

We thank R. Ando, N. Shimakura, T. Nakatani, and M. Toyosawa for their technical support. We also thank Mr. Brent Bell for reading our manuscript. This work was supported by Grants-in-Aids for Scientific Research from the Japanese Ministry of Health, Labor and Welfare.

Appendix A. Supplementary data

Supplementary data associated with this article can be found, in the online version, at doi:10.1016/j.neures.2011.10.005.

References

Adams-Graves, P., Kedar, A., Koshy, M., Steinberg, M., Veith, R., Ward, D., Crawford, R., Edwards, S., Bustrack, J., Emanuele, M., 1997. RheothRx (poloxamer 188) injection for the acute painful episode of sickle cell disease: a pilot study. Blood 90, 2041–2046.

Aoki, M., Liu, J., Richard, I., Bashir, R., Britton, S., Keers, S.M., Oeltjen, J., Brown, H.E., Marchand, S., Bourg, N., Beley, C., McKenna-Yasek, D., Arahata, K., Bohlega, S., Cupler, E., Illa, I., Majneh, I., Barohn, R.J., Urtizberea, J.A., Fardeau, M., Amato, A., Angelini, C., Bushby, K., Beckmann, J.S., Brown Jr., R.H., 2001. Genomic organization of the dysferlin gene and novel mutations in Miyoshi myopathy. Neurology 57, 271–278.

Bansal, D., Miyake, K., Vogel, S.S., Groh, S., Chen, C.C., Williamson, R., McNeil, P.L., Campbell, K.P., 2003. Defective membrane repair in dysferlin-deficient muscular dystrophy. Nature 423, 168–172.

Bashir, R., Britton, S., Strachan, T., Keers, S., Vafiadaki, E., Lako, M., Richard, I., Marchand, S., Bourg, N., Argov, Z., Sadeh, M., Mahjneh, I., Marconi, G., Passos-Bueno, M.R., Moreira Ede, S., Zatz, M., Beckmann, J.S., Bushby, K., 1998. A gene related to Caenorhabditis elegans spermatogenesis factor fer-1 is mutated in limb-girdle muscular dystrophy type 2B. Nat. Genet. 20, 37–42.

Bittner, R.E., Anderson, L.V., Burkhardt, E., Bashir, R., Vafiadaki, E., Ivanova, S., Raffelsberger, T., Maerk, I., Hoger, H., Jung, M., Karbasiyan, M., Storch, M., Lassmann, H., Moss, J.A., Davison, K., Harrison, R., Bushby, K.M., Reis, A., 1999. Dysferlin deletion in SJL mice (SJL-Dysf) defines a natural model for limb girdle muscular dystrophy 2B. Nat. Genet. 23, 141–142.

Borgens, R.B., Bohnert, D., Duerstock, B., Spomar, D., Lee, R.C., 2004. Subcutaneous tri-block copolymer produces recovery from spinal cord injury. J. Neurosci. Res. 76, 141–154.

Illa, I., Serrano-Munuera, C., Gallardo, E., Lasa, A., Rojas-Garcia, R., Palmer, J., Gallano, P., Baiget, M., Matsuda, C., Brown, R.H., 2001. Distal anterior compartment myopathy: a dysferlin mutation causing a new muscular dystrophy phenotype. Ann. Neurol. 49, 130–134.

Illarioshkin, S.N., Ivanova-Smolenskaya, I.A., Greenberg, C.R., Nylen, E., Sukhorukov, V.S., Poleshchuk, V.V., Markova, E.D., Wrogemann, K., 2000. Identical dysferlin mutation in limb-girdle muscular dystrophy type 2B and distal myopathy. Neurology 55, 1931–1933.

Keren, A., Tamir, Y., Bengal, E., 2006. The p38 MAPK signaling pathway: a major regulator of skeletal muscle development. Mol. Cell. Endocrinol. 252, 224–230.

Klinge, L., Aboumousa, A., Eagle, M., Hudson, J., Sarkozy, A., Vita, G., Charlton, R., Roberts, M., Straub, V., Barresi, R., Lochmuller, H., Bushby, K., 2010. New aspects on patients affected by dysferlin deficient muscular dystrophy. J. Neurol. Neurosurg. Psychiatry 81, 946–953.

Lee, R.C., River, L.P., Pan, F.S., Ji, L., Wollmann, R.L., 1992. Surfactant-induced sealing of electropermeabilized skeletal muscle membranes in vivo. Proc. Natl. Acad. Sci. U.S.A. 89, 4524–4528.

Liu, J., Aoki, M., Illa, I., Wu, C., Fardeau, M., Angelini, C., Serrano, C., Urtizberea, J.A., Hentati, F., Hamida, M.B., Bohlega, S., Culper, E.J., Amato, A.A., Bossie, K., Oeltjen, J., Bejaoui, K., McKenna-Yasek, D., Hosler, B.A., Schurr, E., Arahata, K., de Jong, P.J., Brown Jr., R.H., 1998. Dysferlin, a novel skeletal muscle gene, is mutated in Miyoshi myopathy and limb girdle muscular dystrophy. Nat. Genet. 20, 31–36.

Maskarinec, S.A., Wu, G., Lee, K.Y., 2005. Membrane sealing by polymers. Ann. N.Y. Acad. Sci. 1066, 310–320.

McClung, J.M., Judge, A.R., Powers, S.K., Yan, Z., 2010. p38 MAPK links oxidative stress to autophagy-related gene expression in cachectic muscle wasting. Am. J. Physiol. Cell Physiol. 298, C542–C549.

Merchant, F.A., Holmes, W.H., Capelli-Schellpfeffer, M., Lee, R.C., Toner, M., 1998. Poloxamer 188 enhances functional recovery of lethally heat-shocked fibroblasts. J. Surg. Res. 74, 131–140.

Murphy, A.D., McCormack, M.C., Bichara, D.A., Nguyen, J.T., Randolph, M.A., Watkins, M.T., Lee, R.C., Austen Jr., W.G., 2010. Poloxamer 188 protects against ischemia-reperfusion injury in a murine hind-limb model. Plast. Reconstr. Surg. 125, 1651–1660.

Ng, R., Metzger, J.M., Claflin, D.R., Faulkner, J.A., 2008. Poloxamer 188 reduces the contraction-induced force decline in lumbrical muscles from mdx mice. Am. J. Physiol. Cell Physiol. 295, C146–C150.

Paradas, C., Llauger, J., Diaz-Manera, J., Rojas-Garcia, R., De Luna, N., Iturriaga, C., Marquez, C., Uson, M., Hankiewicz, K., Gallardo, E., Illa, I., 2010. Redefining dysferlinopathy phenotypes based on clinical findings and muscle imaging studies. Neurology 75, 316–323.

Quinlan, J.G., Wong, B.L., Niemeier, R.T., McCullough, A.S., Levin, L., Emanuele, M., 2006. Poloxamer 188 failed to prevent exercise-induced membrane breakdown in mdx skeletal muscle fibers. Neuromuscul. Disord. 16, 855–864.

Rayavarapu, S., Van der Meulen, J.H., Gordish-Dressman, H., Hoffman, E.P., Nagaraju, K., Knoblach, S.M., 2010. Characterization of dysferlin deficient SJL/J mice to assess preclinical drug efficacy: fasudil exacerbates muscle disease phenotype. PLoS One 5, e12981.

Rosales, X.Q., Gastier-Foster, J.M., Lewis, S., Vinod, M., Thrush, D.L., Astbury, C., Pyatt, R., Reshmi, S., Sahenk, Z., Mendell, J.R., 2010. Novel diagnostic features of dysferlinopathies. Muscle Nerve 42, 14–21.

Saito, H., Suzuki, N., Ishiguro, H., Hirota, K., Itoyama, Y., Takahashi, T., Aoki, M., 2007. Distal anterior compartment myopathy with early ankle contractures. Muscle Nerve 36, 525–527.

Serbest, G., Horwitz, J., Jost, M., Barbee, K., 2006. Mechanisms of cell death and neuroprotection by poloxamer 188 after mechanical trauma. FASEB J. 20, 308–310.

Suzuki, N., Aoki, M., Hinuma, Y., Takahashi, T., Onodera, Y., Ishigaki, A., Kato, M., Warita, H., Tateyama, M., Itoyama, Y., 2005. Expression profiling with progression of dystrophic change in dysferlin-deficient mice (SJL). Neurosci. Res. 52, 47–60.

Suzuki, N., Motohashi, N., Uezumi, A., Fukada, S., Yoshimura, T., Itoyama, Y., Aoki, M., Miyagoe-Suzuki, Y., Takeda, S., 2007. NO production results in suspension-induced muscle atrophy through dislocation of neuronal NOS. J. Clin. Invest. 117, 2468–2476.

Takahashi, T., Aoki, M., Tateyama, M., Kondo, E., Mizuno, T., Onodera, Y., Takano, R., Kawai, H., Kamakura, K., Mochizuki, H., Shizuka-Ikeda, M., Nakagawa, M., Yoshida, Y., Akanuma, J., Hoshino, K., Saito, H., Nishizawa, M., Kato, S., Saito, K., Miyachi, T., Yamashita, H., Kawai, M., Matsumura, T., Kuzuhara, S., Ibi, T., Sahashi, K., Nakai, H., Kohnosu, T., Nonaka, I., Arahata, K., Brown Jr., R.H., Itoyama, Y., 2003.